




## Article

# Sensitivity Analysis of the Catalytic Ozonation under Different Kinetic Modeling Approaches in the Diclofenac Degradation

José Antonio Lara-Ramos <sup>1,2</sup>, Miguel A. Figueroa Angulo <sup>3</sup>, Fiderman Machuca-Martínez <sup>1</sup>  
and Miguel A. Mueses <sup>3,\*</sup>

<sup>1</sup> Escuela de Ingeniería Química, Universidad del Valle, A.A. 25360 Cali, Colombia; jalarar@itsa.edu.co (J.A.L.-R.); fiderman.machuca@correounivalle.edu.co (F.M.-M.)

<sup>2</sup> Facultad de Ingeniería, ITSA Institución Universitaria, Cra. 45 No. 48-31 Barranquilla, Colombia; lara.jose@correounivalle.edu.co

<sup>3</sup> Photocatalysis and Solar Photoreactors Engineering, Modeling & Application of AOTs, Department of Chemical Engineering, Universidad de Cartagena, 1382-Postal 195 Cartagena, Colombia; mfigueroaa1@unicartagena.edu.co

\* Correspondence: mmueses@unicartagena.edu.co

**Abstract:** Optimization and sensitivity analysis of the kinetic parameters of the catalytic ozonation process is crucial to improve water treatment, reactor design, and construction. This study evaluated the optimization of the kinetic constants for Diclofenac (DCF) degradation during catalytic ozonation with Goethite (FeOOH, as a catalyst) through different kinetic modeling approaches. A central composite design was used to evaluate the effect of ozone dose and catalyst loading. The results showed that FeOOH did not significantly influence the degradation of DCF, while the reactivity of DCF with ozone was high (with >90% degradations in 20 min). However, the variation in catalyst loading significantly affected TOC removal (>10%) and ozone use, with ozone efficiency in ozone transfer ( $R_U$ ) 5% higher than ozonation. After evaluating the different kinetic models of reaction speed by optimizing kinetic parameters and performing sensitivity analysis for the treatment of DCF by catalytic ozonation, it can be concluded that the addition of FeOOH improved the kinetics of the decomposition of ozone and the yield in the production of hydroxyl radicals.

**Keywords:** diclofenac; reaction kinetics; mechanisms; steady-state approximation; elemental reactions; optimization



**Citation:** Lara-Ramos, J.A.; Figueroa Angulo, M.A.; Machuca-Martínez, F.; Mueses, M.A. Sensitivity Analysis of the Catalytic Ozonation under Different Kinetic Modeling Approaches in the Diclofenac Degradation. *Water* **2021**, *13*, 3003. <https://doi.org/10.3390/w13213003>

Academic Editor: Jiangyong Hu

Received: 15 September 2021

Accepted: 21 October 2021

Published: 26 October 2021

**Publisher's Note:** MDPI stays neutral with regard to jurisdictional claims in published maps and institutional affiliations.



**Copyright:** © 2021 by the authors. Licensee MDPI, Basel, Switzerland. This article is an open access article distributed under the terms and conditions of the Creative Commons Attribution (CC BY) license (<https://creativecommons.org/licenses/by/4.0/>).

## 1. Introduction

Emerging contaminants (ECs) such as pharmaceutical compounds have reached a critical level of presence in the environment [1,2]. Catalytic ozonation, as an advanced oxidation process (AOP), has successfully degraded different pharmaceutical compounds present in water [3–5]. Diclofenac (DCF), a pharmaceutical compound with high solubility, complex adsorption, toxic by-products, and conventional treatments, does not degrade [6,7]. Numerous reports in the literature show high concentrations of DCF in water bodies [7–9]. Therefore, degradation and mineralization of the DCF is the object of study using AOP [6,10–12].

The fundamental parameters have been studied in various research works, such as catalyst loading, ozone dosage, and reactor design [11–13]. Therefore, operating variables, catalytic activity, mineralization, and size of reactors have improved significantly [1,4,13,14]. For example, to increase the efficiency of these parameters, the use of a modified flotation cell has recently been proposed as a reactive system. This is used at an industrial level to facilitate dense particle suspension and gas bubble dispersion within the reaction volume [14–17]. In 2019, Lara-Ramos et al. investigated this idea, where the intensification of the advanced oxidation system by  $O_3/TiO_2/UV$  in a flotation cell was executed, leading to cost reduction, and more minor limitations by mass transfer were highlighted [6].

Furthermore, Iron-based catalysts such as Goethite (FeOOH) have been widely accepted for use in catalytic ozonation because of their abundance in nature, ease of synthesis, and low toxicity [14,18–20]. In addition, FeOOH has a high density of hydroxyl radicals on its surface that can attack the contaminant more efficiently. Recent literature reviews have noted how this effect generally increases the rate of contaminant degradation compared to ozonation in the absence of FeOOH [14,21]. Although the previous investigations have allowed reaching a new level of maturity for the degradation of Ecs, the next step is to model and optimize catalytic ozonation [22]. However, this step is more difficult to achieve due to the complexity of the reaction mechanism depending on the evaluated system. For each catalytic ozonation case study, its reaction mechanism is unique in how the catalyst interacts with the targeted organic compounds and with ozone [23].

The nature of the interactions that occur on the surface of FeOOH continues to be debated by researchers, since it is not easy to define the reaction mechanism for catalytic ozonation [20]. However, recent research has described the reaction mechanism of catalytic ozonation with using FeOOH as a catalyst resulting in the highly efficient promotion of hydroxyl radicals as well as the possibility of the direct degradation of contaminants taking place on the catalyst surface [17–20].

Table 1 summarizes some research on kinetic modeling of the catalytic ozonation process for the treatment of water (contaminated with ECs). At the end of the 20th century, most of the research on kinetic modeling focused on well-known and straightforward compounds to study the fundamental kinetic steps of catalytic ozonation [24,25]. These approaches were widespread and are still used today to describe wastewater treatment kinetics due to the matrix of compounds [8,26]. Finally, progress has been made, and there is mature research on new reactor designs [14,27,28] and catalysts [22,24,29,30].

The kinetic modeling of reaction mechanisms has made significant progress in the description of water treatment with ozone. Among the most significant advances are evaluating ECs mixtures [24,25] and including the hydrodynamic effects of new couplings or reactor designs in the reaction mechanism [14,27,28,31–34]. The study and determination of the reaction rate constants are essential to describe the phenomenology of chemical processes. In the last decade, catalytic ozonation has aroused interest as the chemical process for treating ECs, but first it is necessary to have rate constants for the catalytic activity of catalysts such as FeOOH.

Based on the above, in the present work, different approaches for the kinetic modeling of the reaction rate of the ozonation and catalytic ozonation processes were optimized, studied, and compared. In addition, the degradation, mineralization, and  $R_U$  were evaluated in the treatment of DCF with the ozonation and catalytic ozonation processes.

**Table 1.** Recent works are relevant to catalytic ozonation with FeOOH of diclofenac.

System	Source						
	Andreozzi et al. (2001) [35]	Pocostales et al. (2011) [22]	Khataee et al. (2016) [36]	Yao, Hui & Hui. (2017) [23]	Aghaeinejad-Meybodi et al. (2018) [27]	Guo et al. (2019) [24]	Du, Chen & Lin. (2019) [25]
Type of WW	Synthetic	Industrial	Synthetic	Gaseous	Synthetic	Synthetic	Synthetic
Complexity	Low	High	Low	None	Low	Medium	Medium
Contaminant	Oxalic Acid	Diclofenac, sulfametoxazole and 17 $\alpha$ -ethynilstradiol	Nalidixic acid	Toluene	Fluoxetine	diclofenac, gemfibrozil, bezafibrate, etc.	Ibuprofen and acetyl-sulfamethoxazole
Catalyst	MnO <sub>2</sub>	$\gamma$ -Al <sub>2</sub> O <sub>3</sub> & Co <sub>3</sub> O <sub>4</sub> /Al <sub>2</sub> O <sub>3</sub>	Clinoptilolite nanorods	MnO <sub>2</sub> /Graphene	nano- $\gamma$ -alumina	$\alpha$ - or $\beta$ - MnO <sub>2</sub>	multi-walled carbon nanotubes
Reactor type	semi-batch reactor	Fixed-bed reactor	Semi-batch Pyrex reactor	Tube fixed-bed micro-reactor	Semi-batch bubble column reactor	Airtight acrylic column reactor	Unknown
Model nature	Deactivable sites kinetic model	Two-stage first-order model	Pseudo-steady state, empirical law, and artificial neural network	Langmuir-Hinshelwood dual-site	Artificial neural networks	Pseudo-second order	Pseudo-second order
Model adjustment	Visually good	Visually good	0.98, 0.998, 0.991	0.9175	96.8% or 0.983	0.951–0.979	Unknown
Caveats	None	Model needs COD removal calculations	None	Model was fitted with enthalpy and entropy constraints	96.14% removal efficiency was achieved	Assumes oxidation mainly by O <sub>3</sub> and OH <sup>•</sup> , other means negligible	Global parameter approximations

## 2. Materials and Methods

### 2.1. Materials and Reagents

Diclofenac sodium salt ( $C_{14}H_{10}C_{12}NNaO_2$ , >98% HPLC area) and iron (III) hydroxide oxide (Goethite, catalyst grade) were purchased from Sigma-Aldrich (Milwaukee, WI, USA). Drinking tape water from Cali-Colombia was used for all the experimental trials (physicochemical properties in Appendix A, Table A1).

### 2.2. Experimental Equipment

A Flotation Cell (FC, Denver type D-12 manufactured by METSO) was used for all experimental tests. The FC had a stirring speed variation between 0 and 3000 rpm and a reaction tank with a capacity of 2.3 L. In addition, an A2Z Model 5GLAB ozonizer with a maximum capacity of 5000 mg/h was used (see Figure A1 in Appendix A). The determination of ozone in the gaseous phase was carried out by means of an online ozone meter (MINI-HICON, IN USA, San Diego, CA, USA), and the effluent gases were destroyed with a 10% *v/v* KI solution. Meanwhile, some properties of the cell and ozonator are shown in Table A2 of the Appendix A.

### 2.3. Experimental Procedure

The ozonation and catalytic ozonation tests with Goethite were carried out in a reaction volume of 2 L, 1500 rpm, neutral pH, 30 mg/L of DCF, at conditions of 28 °C and 1015 hPa. There was no temperature control, but a variation of  $\pm 0.4$  °C was recorded for the 15 tests during the temperature monitoring. For the ozone dose and catalyst load, a central composite design (CCD) was used, where the FeOOH load was varied between 0.196 to 0.904 g/L, and the variation of the ozone dose was between 1.4 and 7.2 mg/L (see Figure A1 in Appendix A). Additionally, four catalytic ozonation tests were carried out where ozone was kept constant (4.3 mg/min) and the FeOOH load was varied (between 0.1–1 g/L), and two ozonation tests (doses of 4.3–6.3 mg/min) were performed without the presence of a catalyst.

In the ozonation tests, a DCF solution (30 mg/L) was added to the reaction tank, a stirring speed of 1500 rpm was used, and the ozonator was turned on, adjusting the desired ozone dose. The reaction time was 20 min. For catalytic ozonation tests, only the above procedure was followed after adding the load of FeOOH and stirring at 1500 rpm for 10 min, then turning on the ozonator. The reactions between ozone and diclofenac stopped by adding sodium thiosulfate at 0.1 N to the sample. Finally, these were filtered using a Celltreat PVDF/L needle filter (millipore, 0.22  $\mu$ m).

### 2.4. Analytical Monitoring

The diclofenac concentration in each sample of the different tests performed was obtained with a UHPLC (UHPLC Dionex UltiMate 3000 equipped with a dual quaternary pump, WPS3000SL autosampler, and DAD-3000 (RS) diode array detectors). The stationary phase was a Hypersil Green PAH column (5  $\mu$ m, 150 mm  $\times$  4.6 mm) and the mobile phase consisted of 60% acetonitrile and 40% formic acid at 0.1 M. The detection wavelength was 276 nm, and the flow was 0.2 mL/min. Finally, the ozone concentration was measured online using a Mini-Hicon IN-USA ozone analyzer (IN USA., San Diego, CA, USA).

### 2.5. Model Description

#### 2.5.1. Mechanisms of Catalytic Ozonation

The presence of FeOOH as a catalyst in the ozonation process changes the oxidation mechanism of ozonation alone (prevalence of direct and selective ozone attack, R1). In addition, the Goethite surface provides active sites that improve OH $\bullet$  generation. Hydroxyl radicals non-selectively degrade (R2) and enhance DCF mineralization.

Table 2 shows the mechanism of elemental reactions for the catalytic ozonation process. Firstly, the homogeneous ozone decomposition begins with reactions involving hydroxyl ions, perhydroxyl (HO $_2^-$ ), radical superoxide anion (O $_2^- \bullet$ ), namely reactions R3–R6. Then,

intermediate species, such as perhydroxyl radical ( $\text{HO}_2^\bullet$ ), radical oxygen anion ( $\text{O}^{\bullet-}$ ), superoxide radical anion, and ozonide radical ( $\text{O}_3^{\bullet-}$ ), react to form the hydroxyl radical (see reactions R5–R10).

Secondly, from R11 to R16, the mechanism of the heterogeneous decomposition reactions of ozone on the surface of Goethite is described. The catalytic activity begins with the arrival of  $\text{O}_3$  (dipole agent) to the surface of  $\text{FeOOH}$  (with electrophilic H and a nucleophilic O), where ozone binds to  $\text{OH}^-$  on Goethite and  $\text{HO}_2^-$  is formed, which then reacts with more  $\text{O}_3$  to produce  $\text{OH}^\bullet$ . Finally, the water molecule is adsorbed and dissociated to cover the vacancy of the Fe(III) site on  $\text{FeOOH}$  [37]. Thirdly, the reactions of R17–R20 occur, where intermediate species can react and produce  $\text{OH}^\bullet$  or even ozone (adsorbed-R20 or dissolved-R1).

**Table 2.** Heterogeneous catalytic elementary reactions in ozonation with Goethite [5,20,38,39].

No	Elemental Reaction	Reaction Rate Constant
	Direct Reaction	
R1	$\text{O}_3 + \text{DCF} \xrightarrow{k_{\text{O}_3}} \text{P}(\text{intermediarios o } \text{CO}_2)$	$6.0 \cdot 10^7 \text{ M}^{-1} \text{ min}^{-1}$
	Indirect reaction	
R2	$\text{OH}^\bullet + \text{DCF} \xrightarrow{k_{\text{OH}^\bullet}} \text{P}(\text{intermediarios o } \text{CO}_2)$	$4.5 \cdot 10^{11} \text{ M}^{-1} \text{ min}^{-1}$
	Homogeneous decomposition	
R3	$\text{O}_3 + \text{OH}^- \xrightarrow{k_1} \text{HO}_2^- + \text{O}_2$	$4.2 \cdot 10^3 \text{ M}^{-1} \text{ min}^{-1}$
R4	$\text{O}_3 + \text{HO}_2^- \xrightarrow{k_2} \text{HO}_2^\bullet + \text{O}_3^{\bullet-}$	$1.32 \cdot 10^8 \text{ M}^{-1} \text{ min}^{-1}$
R5	$\text{HO}_2^\bullet \xrightleftharpoons[k_{-3}]{k_3} \text{O}_2^{\bullet-} + \text{H}^+$	$k_3 = 4.74 \cdot 10^7 \text{ M}^{-1} \text{ min}^{-1}$ $k_{-3} = 3.0 \cdot 10^{12} \text{ M}^{-1} \text{ min}^{-1}$
R6	$\text{O}_3 + \text{O}_2^{\bullet-} \xrightarrow{k_4} \text{O}_3^{\bullet-} + \text{O}_2$	$9.6 \cdot 10^{10} \text{ M}^{-1} \text{ min}^{-1}$
R7	$\text{O}_3 + \text{OH}^\bullet \xrightarrow{k_5} \text{HO}_2^\bullet + \text{O}_2$	$1.8 \cdot 10^{11} \text{ M}^{-1} \text{ min}^{-1}$
R8	$\text{HO}_2^- + \text{OH}^\bullet \xrightarrow{k_6} \text{HO}_2^\bullet + \text{OH}^-$	$4.5 \cdot 10^{11} \text{ M}^{-1} \text{ min}^{-1}$
R9	$\text{O}_3^{\bullet-} \xrightleftharpoons[k_{-7}]{k_7} \text{O}_2 + \text{O}^{\bullet-}$	$k_7 = 1.26 \cdot 10^3 \text{ min}^{-1}$ $k_{-7} = 1.98 \cdot 10^9 \text{ M}^{-1} \text{ min}^{-1}$
R10	$\text{O}^{\bullet-} + \text{H}_2\text{O} \xrightleftharpoons[k_{-8}]{k_8} \text{OH}^\bullet + \text{OH}^-$	Unknown
	Heterogeneous decomposition	
R11	$\text{FeOOH} + \text{O}_3 \xrightleftharpoons[k_{-9}]{k_9} \text{FeOOH}(\text{O}_3)$	Unknown
R12	$\text{FeOOH}(\text{O}_3) \xrightleftharpoons[k_{-10}]{k_{10}} \text{Fe}(\text{O})\text{OH} + \text{O}_2$	Unknown
R13	$\text{Fe}(\text{O})\text{OH} + \text{O}_3 + \text{H}_2\text{O} \xrightleftharpoons[k_{-11}]{k_{11}} \text{FeOH} \dots$ $+ \text{OH}^\bullet + \text{O}_2^{\bullet-} + \text{O}_2 + \text{H}^+$	Unknown
R14	$\text{FeOH} + \text{O}_3 \xrightleftharpoons[k_{-12}]{k_{12}} \text{FeOH}(\text{O}_3)$	Unknown
R15	$\text{FeOH} \xrightleftharpoons[k_{-13}]{k_{13}} \text{FeO}^\bullet + \text{HO}_3^\bullet$	Unknown
R16	$\text{FeO}^\bullet + \text{H}_2\text{O} \xrightarrow{k_{14}} \text{FeOH} + \text{OH}^\bullet$	Unknown
	Propagation and termination reactions	
R17	$\text{HO}_3^\bullet \xrightleftharpoons[k_{-15}]{k_{15}} \text{H}^+ + \text{O}_3^{\bullet-}$	$k_{15} = 1.98 \cdot 10^3 \text{ M}^{-1} \text{ min}^{-1}$ $k_{-15} = 3.12 \cdot 10^{12} \text{ M}^{-1} \text{ min}^{-1}$
R18	$\text{HO}_3^\bullet \xrightarrow{k_{16}} \text{OH}^\bullet + \text{O}_2$	$6.6 \cdot 10^6 \text{ min}^{-1}$
R19	$\text{O}_3^{\bullet-} + \text{H}_2\text{O} \xrightarrow{k_{17}} \text{OH}^\bullet + \text{OH}^- + \text{O}_2$	$(1.2\text{--}1.8) \cdot 10^3 \text{ M}^{-1} \text{ min}^{-1}$
R20	$\text{FeOOH}(\text{O}_3) + \text{DCF} \xrightarrow{k_{18}} \text{P}$	Unknown

## 2.5.2. Description of Kinetic Reaction Models

### Pseudo-First-Order Model

The reaction mechanism of the catalytic ozonation process consists of direct and indirect reactions that coincide during the process. Therefore, the DCF degradation can be described as the sum of the two reaction pathways [20]:

$$r_{\text{DCF}} = -\frac{d(\text{DCF})}{dt} = -[k_{\text{O}_3}\text{O}_3 + k_{\text{OH}^\bullet}\text{OH}^\bullet]\text{DCF} \quad (1)$$

where DCF is the concentration of diclofenac in M (mol/L),  $t$  is the reaction time in min,  $k_{\text{O}_3}$  and  $k_{\text{OH}^\bullet}$  are the reaction rate constants for direct (ozone attack, in  $\text{M}^{-1} \text{ min}^{-1}$ ), and indirect (hydroxyl radical attack,  $\text{M}^{-1} \text{ min}^{-1}$ ) reactions, respectively. The pseudo-first-order fit is commonly used to determine the reaction rate in AOPs, assuming that ozone

and hydroxyl radicals are the main pollutants oxidants [5]. So, the oxidation of the DCF compound can be described as the sum of two reaction pathways as follows:

$$r_{\text{DCF}} = -\frac{d(\text{DCF})}{dt} = -k'(\text{DCF}) \quad (2)$$

where  $k'$  is the pseudo-first-order reaction rate constant (in  $\text{min}^{-1}$ ), which is also equal to  $k' = k_{\text{O}_3}\text{O}_3 + k_{\text{OH}\cdot}\text{OH}\cdot$ .

#### Second-Order Model

The ozone reactions with many organic compounds present in water, such as the ozone oxidation of caffeine and ibuprofen, can be described using second-order kinetics [14]. In a second-order reaction, the sum of the exponents in the speed law is equal to two and can be expressed as follows:

$$r_{\text{DCF}} = -\frac{d(\text{DCF})}{dt} = -k''(\text{DCF})^2 \quad (3)$$

where  $k''$  is the pseudo-second-order reaction rate constant (in  $\text{mol}^{-1} \text{min}^{-1}$ ).

#### Mixed Order Reaction Model (MORM)

A combination of the pseudo-first and -second-order reaction kinetics was employed to describe the DCF degradation profiles obtained under the different experimental conditions studied for the ozonation and catalytic ozonation processes. The reaction rate expression for this model is described as:

$$r_{\text{DCF}} = -\frac{d(\text{DCF})}{dt} = -k'(\text{DCF}) - k''(\text{DCF})^2 \quad (4)$$

#### Steady-State Approximation Proposal

When the reaction kinetics of a process have several steps of comparable reaction rates, the step that determines the rate is often not obvious. However, some intermediate species are formed during the reaction steps that are not reactive or product. The steady-state approximation (SSA) assumes that one intermediate in the reaction mechanism is consumed as quickly as it is generated [40]. Thus, its concentration remains the same for the duration of the reaction. The SSA is a method used to derive a rate law and can be expressed as follows.

$$\hat{r}_{\text{Int}\cdot} = \frac{d(\text{Int}\cdot)}{dt} = \sum_{i=1}^n \hat{r}_{i,\text{Int}\cdot} \cong 0 \quad (5)$$

where  $\text{Int}\cdot$  is an intermediate species and  $n$  is the number of reactions where the  $\text{Int}\cdot$  species appears. The mathematical procedure reflecting the SSA resulted in a pair of differential equations describing the DCF degradation and its dependence on the intermediate species generated (see Table 1).

$$r_{\text{DCF}} = -\frac{d(\text{DCF})}{dt} = -k_{\text{O}_3}\text{O}_3 \text{DCF} - k_{\text{OH}\cdot}\text{OH}\cdot\text{DCF} - k_{18} \frac{k_9(\text{FeOOH})\text{O}_3}{k_{-9} + k_{18}\text{DCF}} \text{DCF} \quad (6)$$

However,  $\text{OH}\cdot$  must be found to function only the measured variables: DCF,  $\text{O}_3$ , and FeOOH. Using the reactions R1–R20 to find an expression of only these terms, the following non-linear function was obtained for  $\text{OH}\cdot$ :

$$\frac{d(\text{OH}\cdot)}{dt} = \frac{(\alpha - 3k_4k_{\text{OH}\cdot})\text{O}_3\text{OH}\cdot + (\theta + \beta\text{OH}) \frac{\text{O}_3\text{FeOOH}}{k_{-9} + k_{18}\text{DCF}^2} + \gamma\text{OH}\cdot^2 + \eta\text{O}_3^2}{\omega\text{O}_3^2 + (\delta - \alpha)\text{O}_3\text{DCF} - \lambda\text{O}_3\text{FeOOH} + \mu \frac{\text{O}_3\text{FeOOH}}{k_{-9} + k_{18}\text{DCF}} - \gamma\text{OH}\cdot\text{DCF}} \times r_{\text{DCF}} \quad (7)$$

where  $\alpha = 3k_6k_{\text{O}_3}$ ,  $\beta = 3k_6k_9k_{18}$ ,  $\gamma = 3k_6k_{\text{OH}\cdot}$ ,  $\delta = 3k_2k_{\text{OH}\cdot}$ ,  $\eta = 3k_2k_{\text{O}_3}$ ,  $\lambda = 3k_6k_9$ ,  $\theta = 3k_2k_{18}k_9k_9$ ,  $\mu = \beta/k_{18}$ , and  $\omega = 3k_2k_5$ .

### Proposal Model Based on Elementary Reactions

A kinetic model of elementary reactions was developed where all possible transitory states of intermediate species and their interactions are taken into account, with the final purpose of carrying out a robust analysis of the kinetic constants of the catalytic ozonation process reaction rates. A system of 21 differential equations representing the total order elemental reactions kinetics was obtained and simultaneously solved. Some of these equations are shown in (8–12) as well as the generalized form for any species (see Equation (12)).

$$r_{\text{DCF}} = \frac{\partial(\text{DCF})}{\partial t} = -k_{\text{O}_3}\text{O}_3\text{DCF} - k_{\text{OH}\cdot}\text{OH}\cdot\text{DCF} - k_{18}[\text{FeOOH}\cdot\cdot\cdot(\text{O}_3)]\text{DCF} \quad (8)$$

$$\frac{\partial(\text{O}_3)}{\partial t} = -k_{\text{O}_3}\text{O}_3\text{DCF} - k_1\text{O}_3\text{OH}^- - k_2\text{O}_3\text{HO}_2^- - k_4\text{O}_3\text{O}_2^{\cdot-} - k_5\text{O}_3\text{OH}\cdot - k_9\text{O}_3\text{FeOOH} + k_{-9}[-\text{FeOOH}\cdot\cdot\cdot(\text{O}_3)] \\ k_{11}\text{O}_3\text{FeOOH} + k_{-11}\text{OH}\cdot\text{O}_2^{\cdot-}\text{O}_2\text{H}^+\text{FeOH} - k_{12}\text{O}_3\text{FeOH} + k_{-12}[\text{FeOH}\cdot\cdot\cdot(\text{O}_3)] \quad (9)$$

$$\frac{\partial(\text{OH}\cdot)}{\partial t} = -k_{\cdot}\text{OH}\text{OH}\cdot\text{DCF} - k_5\text{OH}\cdot\text{O}_3 - k_6\text{OH}\cdot\text{HO}_2^- - k_{-8}\text{OH}\cdot\text{OH}^- + k_8\text{O}^{\cdot-} + k_{11}\text{O}_3\text{FeOOH} - k_{-11}\text{OH}\cdot\text{O}_2^{\cdot-}\text{O}_2\text{H}^+\text{FeOH} \\ + k_{14}\text{FeO}\cdot + k_{16}\text{HO}_3^{\cdot} + k_{17}\text{O}_3^{\cdot} \quad (10)$$

$$\frac{\partial(\text{FeOOH})}{\partial t} = -k_9\text{O}_3\text{FeOOH} + k_{-9}\frac{k_9\text{O}_3\text{FeOOH}}{k_{-9} + k_{18}\text{DCF}} \quad (11)$$

$$r_i = \frac{\partial(C_i)}{\partial t} = -\sum_i k_{ij}C_iC_j + \sum_{j,k} k_{j,k}C_jC_k \quad (12)$$

The complete set of equations is described in Appendix A (see Equations (A1)–(A20)). When adjusted, this system of equations requires the remaining twelve unknown kinetic parameters that complete the numerical description of the proposed reaction mechanism, nine of which belong to the new surface reactions for FeOOH.

### General Assumptions for Kinetic Models

In SSA's kinetic modeling approach, it assumes a minimal description of reaction kinetics. Since the number of differential equations and kinetic constants is simplified, this approach assumes a net production rate for the Int• in the reaction mechanism close to or equal to zero. Therefore, in SSA, the reaction rate equations cannot express the reaction mechanism effects in determining the step reaction conditions [40].

The kinetic models of elementary reactions are more fundamental approaches in which the reaction pathways between reactants and their intermediaries are explained in detail. In this type of kinetic model approach, a limited number of assumptions are needed, and the rate parameters are more fundamental in nature [5].

The next assumptions were established to reach the final set: (I) The reaction only occurs in the aqueous phase, and therefore water concentration is constant. (II) The catalytic surface does not suffer significant changes in its optical properties, surface area, and active sites throughout the process. (III) No gaseous phase reactions are considered. (IV) Ozone mass transfer from a gaseous phase to catalyst is negligible. (V) The reaction refers only to the organic substrate without considering the nature of its intermediates. (VI) Perfect mix was assumed for species and pseudo species dissolved in the liquid phase. Additionally, the effects of molecular mass transfer were not considered because the complexity of the system of differential equations was not increased. Furthermore, it can be assumed that ozone diffusion easily transports it to the liquid phase mass.

### 2.5.3. Hatta Number and Ozone Efficiency in Ozone Transfer

Hatta dimensionless number (Ha) establishes the relative importance of the chemical reaction and the mass transfer rates [33]. In addition, the magnitude of Ha allows to define

whether the degradation of a pollutant by oxidation with ozone is in a slow kinetic regime ( $Ha < 0.02$ ), diffusional ( $0.02 < Ha > 0.3$ ), moderate ( $0.3 < Ha < 3$ ), or fast ( $Ha > 3$ ) [14].

$$Ha = \frac{\sqrt{k''D_{O_3}C_0}}{k_L} \tag{13}$$

where  $k''$  is the rate constant of the direct reaction (see Equation (3)) between ozone and the DCF concentration,  $C_0$  is the initial DCF concentration ( $30 \text{ mg/L}$  of DCF =  $1.01 \cdot 10^{-4} \text{ M}$ ),  $D_{O_3}$  is the ozone diffusivity in water, and  $k_L$  is the mass transfer coefficient in the liquid phase. The ozone efficiency in ozone transfer ( $R_U$ ) was expressed as follows [20]. Using  $R_U$ , it is possible to quantify the ozone consumption and the efficiency of ozone utilization for a reactor during ozonation.

$$R_U = \frac{[O_3]_C}{[O_3]_T} \tag{14}$$

where  $[O_3]_T$  is the total concentration of applied ozone and  $[O_3]_C$  is the concentration of ozone consumed (for more information, a detailed description can be found in the methodology of Lara-Ramos et al. [14]).

### 2.5.4. Numerical Optimization Method

For calculating the kinetic rate constants of the reaction of the kinetic models of SSA and elementary reactions, the fourth order Runge–Kutta method (RK4, with an absolute error tolerance of  $10^{-4}$ ) and the algorithm of the direct search for Nelder–Mead (NM). Figure 1 shows the solution algorithm used to fit the kinetic constants of the kinetic model reactions. The implementation and simulation of the kinetic models were carried out in the specialized programming software MATLAB R2020a. Multiple successful direct NM searches were carried out for different initiation vectors and then compared to ensure an adequate minimum objective function value.

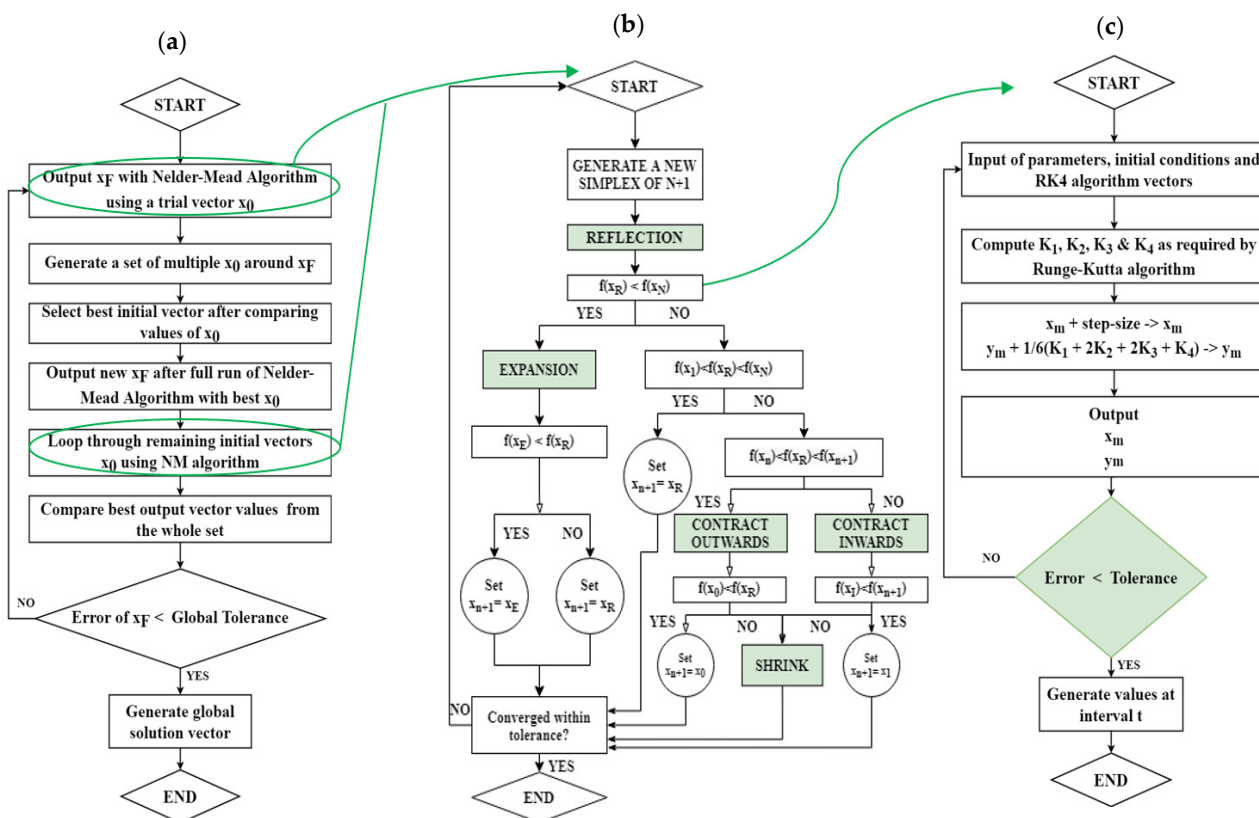


Figure 1. Algorithms for (a) Global search, (b) NM, and (c) RK4.



The key steps of the numerical procedure of the Nelder–Mead algorithm are outlined in green in the algorithm flow diagram (reflection, expansion, contraction, and shrink). In addition, the starting vector ( $X_0$ ) that allowed to define a new vector ( $X_f$ ) during the iterations of steps (n) of the simulation was defined based on the weighted analysis of the average magnitudes of the kinetic constants of the reaction speeds reported in Table 2. Finally, RK4 integration is repeated throughout each NM iteration and whenever there is an objective function value comparison that does not satisfy the tolerance criteria.

After achieving the most suitable parameters with the computer program, a sensitivity analysis was carried out to gauge their confidence values. Finally, using the same algorithm but changing the variable from kinetic parameters to  $[\text{FeOOH}]$  y  $[\text{O}_3]$ , their optimal operational values were optimized with the maximum degradation percentage objective function.

The model used to adjust the kinetic parameters of the degradation reaction are those of non-linear multiparametric optimization, which is based on the evaluation of the standard deviation of the objective function of the global sample to determine the error between the experimental data ( $C_{i,\text{Exp}}$ ) and those calculated ( $C_{i,\text{Cal}}$ ) by the model of Gou et al. [41].

$$F_{\text{obj}} = \sqrt{\frac{1}{N-1} \sum_{j=1}^N \left[ \frac{C_{i,\text{exp}}(C_{ij}^0, C_{m,\text{cat}j}, \dots) - C_{i,\text{cal}}(\alpha_1, \alpha_2, C_{ij}^0, C_{m,\text{cat}j}, \dots)}{C_{i,\text{exp}}(C_{ij}^0, C_{m,\text{cat}j}, \dots)} \right]^2} \quad (15)$$

### 3. Results

#### *Degradation, Mineralization y $R_U$ of DCF*

Figure 2 shows the percentages obtained for the degradation, mineralization, and  $R_U$  of the ozonation and catalytic ozonation processes. The percentages of mineralization and degradation of diclofenac increase with increasing ozone dose for ozonation tests. Meanwhile, for the catalytic ozonation process, the percentage of DCF degradation decreases. This could indicate that the ozone molecule direct attacks decrease due to the heterogeneous ozone decomposition into  $\text{OH}^\bullet$  and homogeneous decomposition in ozonation [14]. The previous behavior in degradation percentages is corroborated by the results of DCF mineralization shown for the tests with a variation of the ozone dose with loads of 0.8 g/L and 0.55 g/L of FeOOH, in which the degradation decreased (<10%) and mineralization percentage increased (~5%).

Furthermore, the results of ozone efficiency in ozone transfer shown in Figure 2 indicate that as the catalyst load increases, ozone consumption increases, as can be seen with 4.3 mg/min of ozone applied and varying FeOOH load of 0.1–1 g/L.  $R_U$  percentages are increased. Therefore, a possible cause of  $R_U$  improvement may be an increase in  $\text{OH}^\bullet$  production due to the catalytic activity of FeOOH in the decomposition of the ozone molecule. Parallel to that, the results obtained for catalytic ozonation in the CCD show that there is a positive effect in the use of ozone (see  $R_U$ ) by increasing the FeOOH load, which translates into higher percentages of mineralization. For example, in a test with  $[\text{O}_3]_T = 4.3$  mg/min and 0.904 g/L of FeOOH, mineralization of 38.6% was obtained, and a  $R_U$  37.21% better in  $R_U$  than the other tests at the same ozone dosage condition.

DCF degradation improves with increasing ozone dose, both for ozonation and catalytic ozonation. Similar results were reported in the following works [6,14]. The mineralization and the  $R_U$  of the catalytic ozonation improved with the increase in the FeOOH load, which would demonstrate that the surface of the Goethite decomposes the ozone into non-selective reactive species such as  $\text{OH}^\bullet$  that increase the mineralization of intermediates (reluctant to ozone attack) [6,42] and  $[\text{O}_3]_C$  in the liquid phase.

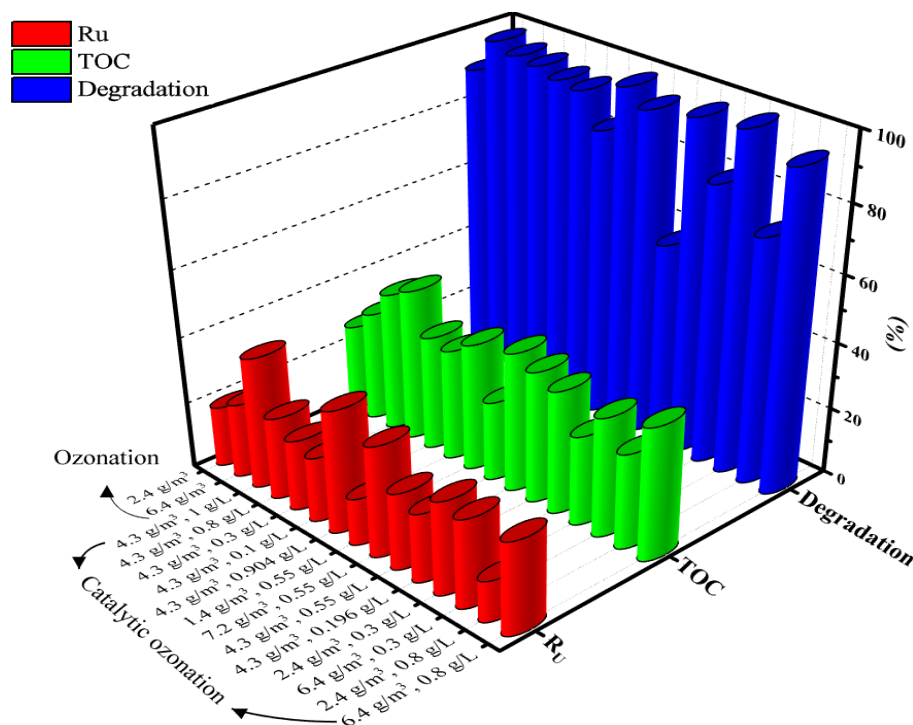


Figure 2. Degradation, mineralization, and  $R_U$  percentages of the DCF through the ozonation and catalytic ozonation processes.

#### 4. Discussion

##### 4.1. Pseudo-First-Order, Second-Order, and MORM Reaction Rate Kinetic Model Fits

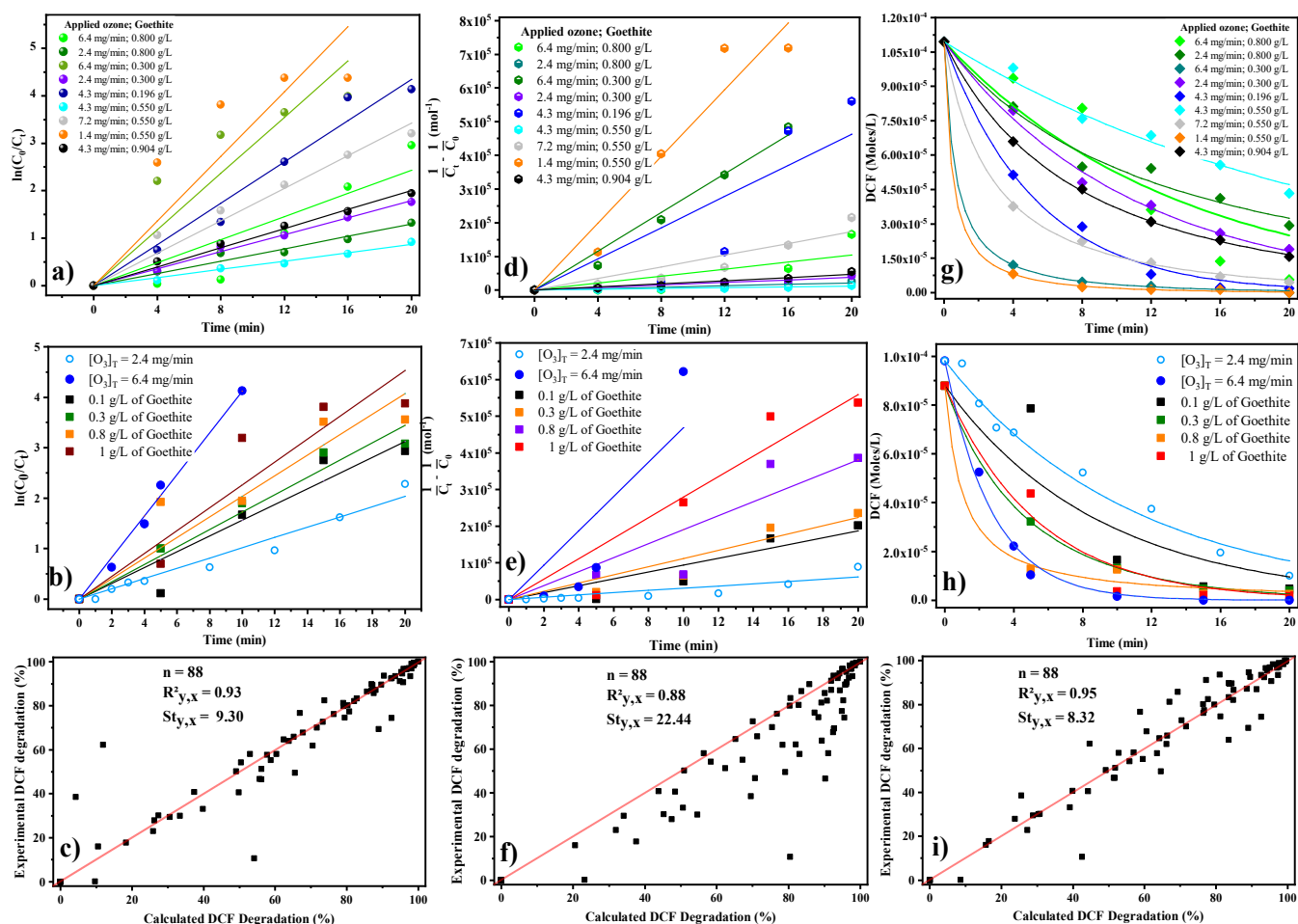
Table 3 shows the reaction rate constants for three kinetic models, their respective correlation coefficient ( $R^2$ ), Hatta, and the reaction kinetic regime for the ozonation and catalytic ozonation processes. For Ha and the kinetic regime, a second-order kinetic model is assumed.

Table 3. Reaction rate constants/ $R^2$  for different reaction models, Hatta and kinetic regime as a function of the process and operating conditions.

Process Operating Conditions		Pseudo-First-Order $k' (\text{min}^{-1})/R^2$	Kinetic Models		Hatta/Kinetic Regime
$[O_3]_T$ (mg/min)	Catalyst Loading (g/L)		Second-Order $k'' (\text{M}^{-1} \text{min}^{-1})/R^2$	MORM $k' (\text{min}^{-1}) - k'' (\text{M}^{-1} \text{min}^{-1})/R^2$	
Ozonation					
2.4	0.0	0.1016/0.98	51.267/0.84	0.0899–6.4429/0.97	0.01/very slow
6.4	0.0	0.4118/0.99	$7.82 \cdot 10^2/0.81$	0.3638–0.0158/0.99	0.03/diffusional
Catalytic ozonation					
4.3	0.1	0.1561/0.96	$1.56 \cdot 10^2/0.93$	0.1108–0.3104/0.84	0.01/very slow
4.3	0.3	0.1721/0.98	$1.86 \cdot 10^2/0.95$	0.1597–7.68 $\cdot 10^2/0.99$	0.01/very slow
4.3	0.8	0.2037/0.96	$3.17 \cdot 10^2/0.92$	0.0171–1.08 $\cdot 10^4/0.99$	0.02/diffusional
4.3	1	0.2266/0.96	$4.65 \cdot 10^2/0.96$	0.1861–0.3711/0.97	0.02/diffusional
6.4	0.8	0.1215/0.91	86.7880/0.74	0.0739–0.2623/0.77	0.01/very slow
2.4	0.8	0.065/0.99	17.8360/0.95	0.0283–5.49 $\cdot 10^2/0.98$	0.005/very slow
6.4	0.3	0.2955/0.95	$4.79 \cdot 10^2/0.99$	0.1214–1.33 $\cdot 10^4/0.99$	0.02/diffusional
2.4	0.3	0.0896/0.99	31.5340/0.97	0.0883–38.21/0.99	0.01/very slow
4.3	0.196	0.2171/0.99	$3.85 \cdot 10^2/0.86$	0.1879–0.0405/0.99	0.02/diffusional
4.3	0.55	0.0435/0.99	9.8636/0.97	0.0407–20.5171/0.98	0.003/very slow
7.2	0.55	0.171/0.99	$1.44 \cdot 10^2/0.93$	0.0807–2.79 $\cdot 10^3/0.99$	0.01/very slow
1.4	0.55	0.3406/0.93	$8.26 \cdot 10^2/0.97$	0.1640–1.88 $\cdot 10^4/0.99$	0.03/diffusional
4.3	0.904	0.1003/0.99	38.9310/0.97	0.0625–7.23 $\cdot 10^2/0.99$	0.01/very slow

In the ozonation process, the reaction rate of diclofenac by direct attacks of the ozone molecule increases significantly with the increase in the dose of ozone applied (see column

four for  $k''$ ). Similarly, the masked contribution of the  $O_3$  and  $OH^\bullet$  attacks represented by  $k'$  (with  $R^2$  closer to 1 than  $k''$ ) increases (see Figure 3b,e,h). As can be seen, the reaction rate constant for the pseudo-first-order increased by 305.31% and the second-order constant by 1425.35% when going from an ozone dose of 4.3 mg/min to 6.3 mg/min. Additionally, the ozone dose increases for ozonation, from a slow kinetic regime ( $Ha = 0.01$ ) to a diffusional one ( $Ha = 0.03$ ) for the tests of 2.4 mg/min and 6.4 mg/min, respectively. Comparable behavior for  $k'$  and  $k''$  were reported for caffeine degradation under similar operating conditions [14,33,34].



**Figure 3.** For ozonation and catalytic ozonation: prediction of experimental data using pseudo-first-order (a,b), second-order models (d,e), MORM (d,g,h), and correlation with calculated data (c,f,i).

The increase in the  $FeOOH$  load in the catalytic ozonation significantly improved the attacks of  $O_3$  and  $OH^\bullet$  on the DCF molecules (see in Table 3 tests with  $[O_3]_T = 4.3$  mg/min with the variation of  $FeOOH$  from 0.1 g/L to 1 g/L), based on the values shown in Sections 3 and 4 for the reaction constants  $k'$  and  $k''$ , with a suitable data correlation for both constants (see  $R^2$  and Figure 3). Meanwhile, it is important to note that CCD tests with low catalyst loading have high values of second-order reaction rate constants, which could mean that direct oxidation (attacks by  $O_3$ ) and indirect oxidation by  $OH^\bullet$  predominate, as can be seen in Figure 2.

On the other hand, there is no direct relationship between the catalyst load and the kinetic regime, which is related to the low  $Ha$  values for the catalytic ozonation of DCF. Finally, the literature has demonstrated the positive effect of the  $FeOOH$  catalytic activity on ozone decomposition and the mineralization of organic pollutants [14,33,39,42,43].

Figure 3 shows the prediction of experimental data from the CCD for the catalytic ozonation process for the kinetic models of the reaction rate of the pseudo-first-order model

(a), second-order model (d), and MORM (g). The fit of the three kinetic models is acceptable for the CCD data, based on the standard deviation ( $St_{x,y}$ ) and correlation of experimental and calculated data (see Figure 3c,f,i). However, in the test with  $[O_3]_T = 6.4$  mg/min and 0.8 g/L of FeOOH, both the second-order model and MORM did not adjust their data. This test is closer to the pseudo-first-order model ( $R^2 = 0.91$  and seen Figure 3c), which indicates a masked oxidation effect between  $O_3$  and  $OH^\bullet$ . Meanwhile, the MORM showed a higher correlation for some tests ( $R^2 = 0.99$  and seen Figure 3i) than the individual models, such as  $[O_3]_T = 4.3$  mg/min and  $[O_3]_T = 1.4$  mg/min with 0.196 g/L of FeOOH and 0.55 g/L of FeOOH, respectively. The MORM describes the masked attacks of the different oxidant species ( $k'$ ) [22,44] and direct ozone attacks ( $k''$ ) [24,25].

The ozonation tests (for  $[O_3]_T = 2.4$  mg/min and 6.4 mg/min) and catalytic ozonation tests under the conditions of  $[O_3]_T = 4.3$  mg/min and variation of the catalyst load from 0.1 g/L to 1 g/L of FeOOH are shown in Figure 3b,e,h). Firstly, the fits (see Table 3) and prediction data for ozonation are higher for the pseudo-first-order kinetic models and model MORM than for the second-order model, for which a better correlation and estimation of data can be obtained. However, Beltran et al. [45] found that DCF reacted almost everything with ozone with a molar ratio of ~8:1. Secondly, the prediction of trends and correlation for the catalytic ozonation tests increases with FeOOH loading for the second and MORM kinetic models, while for the pseudo-first-order model, the correlation remains constant ( $R^2 = \sim 0.9$ ). Finally, the approximations of kinetic models of pseudo-first-order, second-order, and MORM between them are subject to the evaluated operational conditions and do not differentiate between direct and indirect oxidation of the DCF. Additionally, these parameters do not have the phenomenological significance of the two evaluated processes.

#### 4.2. Steady-State Approximation Proposal

Table 4 shows the optimized values for the kinetic constants of the reaction rate for the SSA model. It is essential to point out that the SSA model pseudo parameters encompass some of the literature values (shown in Table 2). Therefore, the constants of the elemental reactions are broken down and shown in Table 4. Meanwhile  $k_2$ ,  $k_5$  y  $k_6$  remained in the magnitude and order of their theoretical counterpart proposed by Beltran et al. [5] and Hoigné et al. [46].

**Table 4.** Reaction rate constants for the SSA kinetic model.

Parameter ( $M^{-1} \text{ min}^{-1}$ )	Value
Direct ozone attacks ( $k_{O_3}$ )	$6.97 \times 10^2$
Hydroxyl radical attacks ( $k_{OH^\bullet}$ )	$2.02 \times 10^{11}$
Ozone adsorption on FeOOH ( $k_9$ )	$4.59 \times 10^3$
Ozone desorption ( $k_{-9}$ )	$2.00 \times 10^7$
Adsorbed ozone attacks ( $k_{18}$ )	$8.60 \times 10^7$

The magnitude of the reaction constants for direct and indirect oxidation are different from those reported by Hoigné et al. [46] (see R1 and R2 in Table 2). As can be seen in the case of indirect oxidation  $k_{OH^\bullet}$ , a magnitude of  $2.02 \times 10^{11}$  was obtained compared to  $4.5 \times 10^{11}$ . For direct oxidation,  $k_{O_3}$  had a difference in the order of  $10^5$  between the refueled and the calculated value. Due to the characteristics of the process and the experimental conditions, these two reaction kinetic constants are fundamental to give a partial description of the catalytic ozonation process's adequate phenomenology. Therefore, it is necessary to carry out a sensitivity analysis.

Meanwhile, the above differences could be explained by considering that the system studied by Hoigné et al. [24] corresponds to the ozonation of diclofenac without a catalyst. Although both systems use ozone, the inclusion of Goethite in the reactive system and how it interacts with ozone completely change the reaction system and mechanism.

On the other hand, the DCF degradation by attacks of  $O_3$  molecules transferred to the Goethite surface by adsorption is represented by the reaction constant  $k_{18}$ . The reaction rate constant  $k_{18}$  is 123,385.94 times the value of  $k_{O_3}$ , from which the above two hypotheses can be proposed. Firstly, the FC promotes the contact of the ozone bubbles with the catalyst particles [47,48]. Secondly, some of the ozone contained in the bubbles that interact with FeOOH can adsorb onto the catalyst surface [33]. Finally, the adsorbed ozone can participate in DCF degradation by direct attacks or indirect oxidation through the formation of  $OH^\bullet$  ( $O_3$  decomposition) [6,14].

Figure 4 shows the experimental data prediction (ozonation and catalytic ozonation), calculated  $OH^\bullet$ , and data correlation for the proposed SSA kinetic model. The trends for the experimental data shown in Figure 4a,b indicate that the SSA model adequately predicts most tests for ozonation and catalytic ozonation. However, the tests with a catalyst load greater than or equal to 0.550 g/L of FeOOH and ozone doses greater than 4.3 mg/min present scattered data from the trend lines proposed by the SSA model. This decreases the correlation between the data and increases the standard deviation of the SSA model (see Figure 4d). As an example of the previous results, we can mention the tests with a catalyst load of 0.800 g/L and 0.550 g/L, with ozone doses of 6.4 mg/min and 7.2 mg/min, respectively.

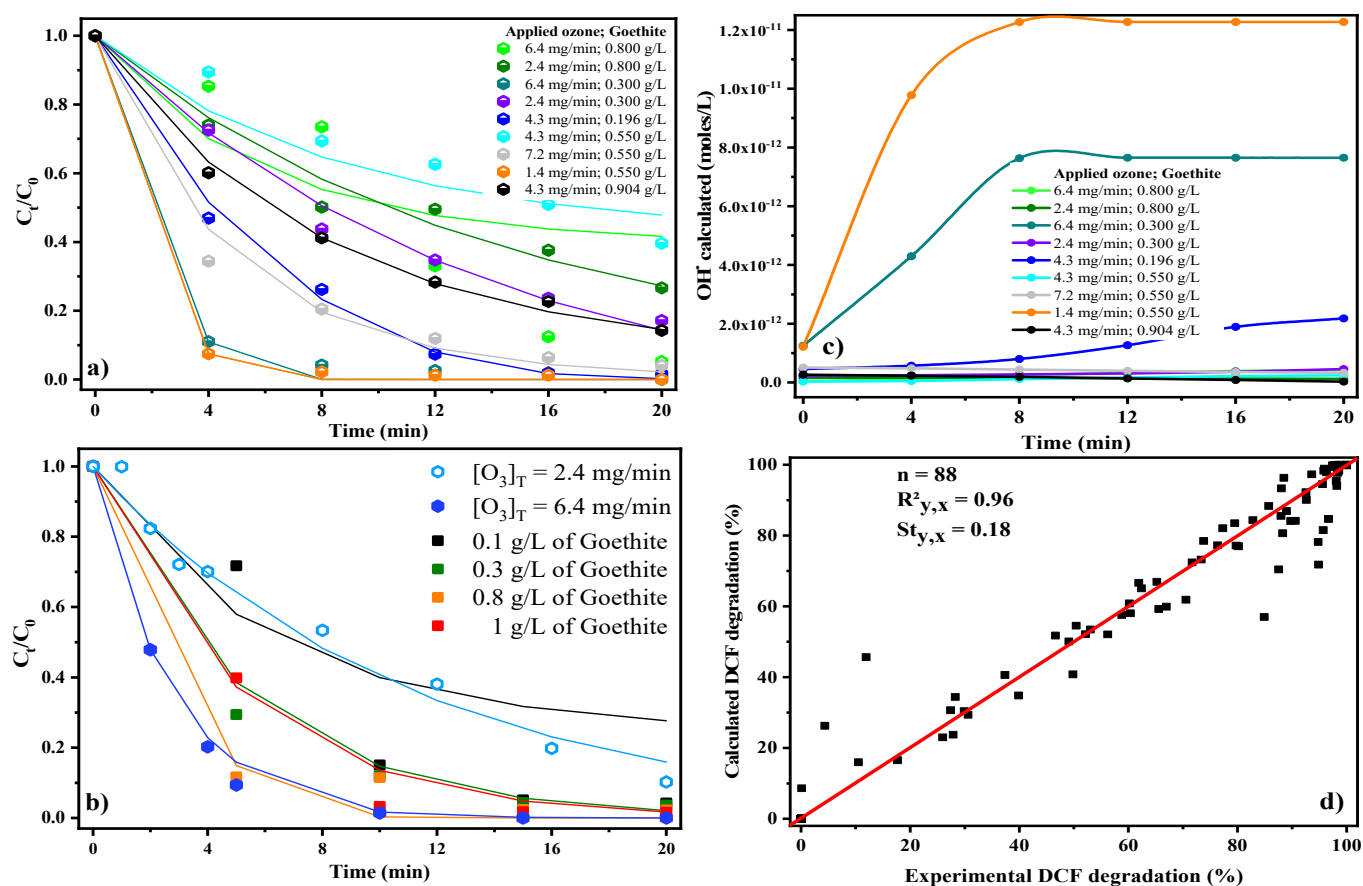


**Figure 4.** Prediction of experimental data using the SSA kinetic model for ozonation and catalytic ozonation (a,b), moles of  $OH^\bullet$  calculated (by SSA) (c), and correlation of experimental and calculated data (d).

Figure 4c shows the generation of  $OH^\bullet$  calculated based on the SSA kinetic model and based on the theoretical trends presented for catalytic ozonation. As can be seen, for low ozone doses ( $<3$  mg/min) and catalyst concentrations above 0.5 g/L, FeOOH increases the generation of  $OH^\bullet$ , and after 8 min of operation, the concentration of hydroxyl radicals stabilizes (the catalytic activity on ozone reaches the stable state). This is because the FeOOH catalyst provides the active sites on which ozone decomposition occurs. Therefore, the

higher the concentration of the catalyst, the greater the number of active sites. Meanwhile, this increase may favour other intermediate steps for a high ozone dose (>4 mg/min). However, the SSA kinetic model is limited in predicting intermediate steps and species.

The percentage correlation ( $R^2 = 0.96$ ) and percentage standard deviation ( $St_{y,x} = 0.18$ ) of calculated and experimental data obtained through the SSA model allow us to infer an adequate prediction compared to the second-order kinetic model for trends in reaction rate for DCF degradation, by ozonation and catalytic ozonation processes (see Figure 4d).

The crucial advantage of SSA is that fewer reaction kinetic constants are required to describe the ozonation and catalytic ozonation process's reaction rates. In contrast, the disadvantage of SSA is a more limited description of the reaction mechanism. Additionally, the reaction mechanism dynamics cannot be described over time since they cannot account for the changes in the intermediate steps that could be important for the catalytic ozonation process as a function of the change in reaction conditions [40].

#### 4.3. Degradation, Mineralization y $R_U$ of DCF

Table 5 shows the optimization of the parameters or kinetic constants corresponding to the PBRE model for ozonation and catalytic ozonation. The kinetic constants of reaction rate with the highest numerical magnitude belong to reactions where  $\text{OH}^\bullet$  has been generated ( $4.10 \times 10^{10} \text{ M}^{-1} \text{ min}^{-1}$ ) or related to its generation (see kinetic constants of  $\text{FeOOH}$ ).

**Table 5.** Reaction rate constants for the SSA kinetic model.

Parameter ( $\text{M}^{-1} \text{ min}^{-1}$ )	Value	Parameter ( $\text{M}^{-1} \text{ min}^{-1}$ )	Value
Direct ozone attacks ( $k_{\text{O}_3}$ )	$2.55 \times 10^3$	$\text{OH}^\bullet$ generation on the $\text{FeOOH}$ surface ( $k_{11}$ )	$2.12 \times 10^9$
Hydroxyl radical attacks ( $k_{\text{OH}^\bullet}$ )	$4.10 \times 10^{10}$	Parasitic reaction on $\text{OH}^\bullet$ ( $k_{-11}$ )	$5.49 \times 10^2$
$\text{OH}^\bullet$ generation by $\text{H}_2\text{O}$ and $\text{O}^{\bullet-}$ ( $k_8$ )	$4.92 \times 10^{13}$	$\text{O}_3$ adsorption on $\text{FeOH}$ ( $k_{12}$ )	$5.86 \times 10^9$
Parasitic reaction on $\text{OH}^\bullet$ ( $k_{-8}$ )	$8.32 \times 10^7$	$\text{O}_3$ desorption on $\text{FeOH}$ ( $k_{-12}$ )	74.03
Ozone adsorption on $\text{FeOOH}$ ( $k_9$ )	$5.95 \times 10^7$	Generation of hydrogen trioxy radical ( $k_{13}$ )	$4.06 \times 10^6$
Ozone desorption ( $k_{-9}$ )	$4.29 \times 10^{10}$	Hydrogen trioxy radical decomposition ( $k_{-13}$ )	$7.25 \times 10^2$
$\text{O}_3$ decomposition into oxygen ( $k_{10}$ )	$1.96 \times 10^9$	$\text{OH}^\bullet$ generation on the $\text{FeOOH}$ surface ( $k_{14}$ )	0.16
$\text{O}_3$ generation ( $k_{-10}$ )	0.667	Adsorbed ozone attacks ( $k_{18}$ )	$1.90 \times 10^8$

The adjusted value for the PBRE model of the reaction rate constant for the direct attacks of the ozone molecule on the DCF is comparable or greater by one or two orders of magnitude in the power of ten than the values reported in the literature [6,49,50]. However, it is lower in three order magnitudes in the power of ten than reported in Table 2. Similarly, the adjusted value for the indirect oxidation reaction cost of DCF is similar to that reported in the following works [1,49,50].

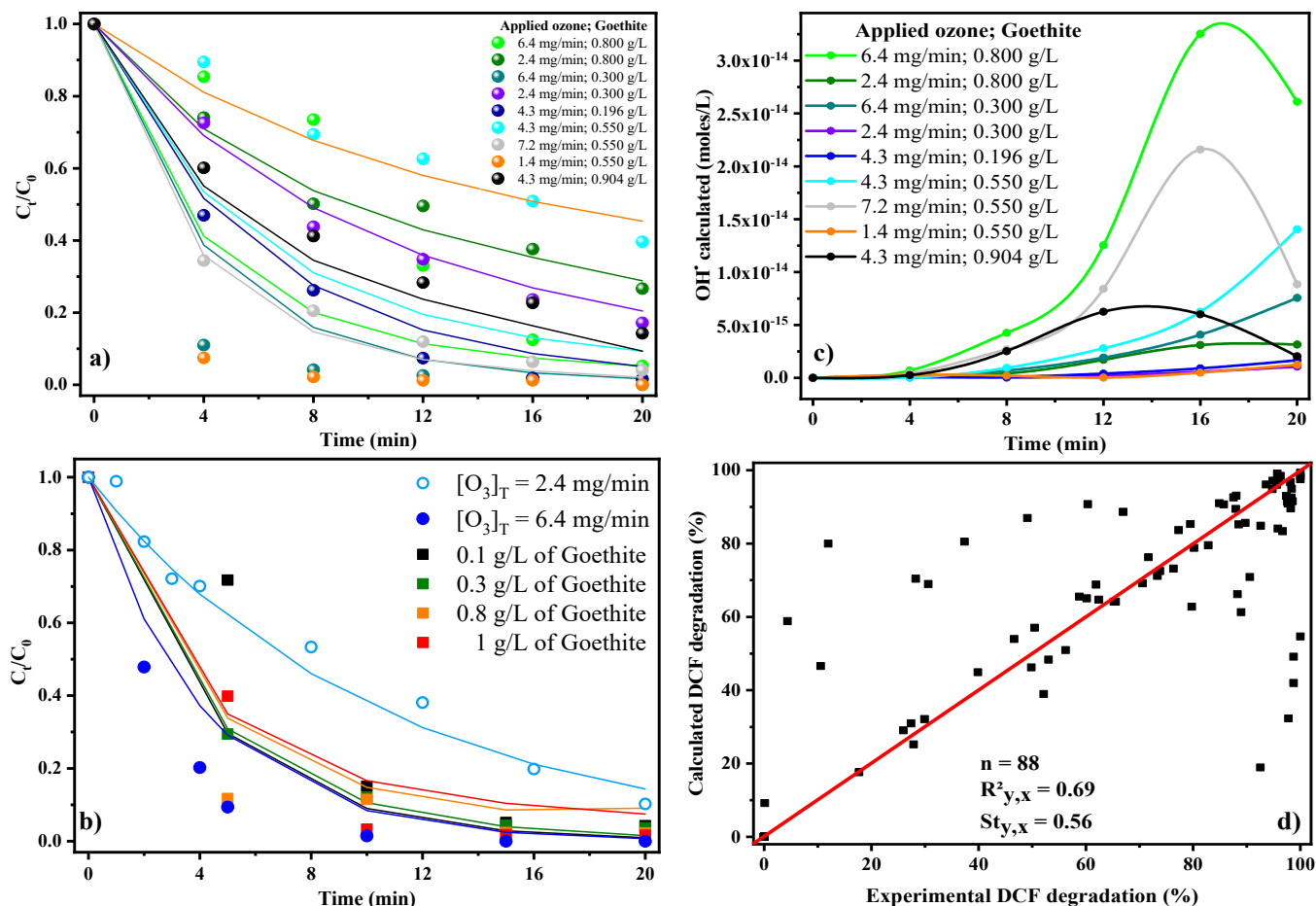
Meanwhile, the adjusted values for the kinetic rate constants related to  $\text{FeOOH}$  and the generation of  $\text{OH}^\bullet$  have relatively high numerical values, except for the kinetic constant for the surface generation of  $\text{OH}^\bullet$  (see  $k_{14}$ ). Thus, the adjustment of the reaction constants involving  $\text{FeOOH}$  indicates an important catalytic activity of this catalyst.

Figure 5 shows the experimental data prediction (ozonation and catalytic ozonation), calculated  $\text{OH}^\bullet$ , and data correlation for the kinetic model of elemental reactions.

The trends for the experimental data are shown in Figure 5a,b indicate that the PBRE model predicts the experimental data less satisfactorily than the SSA model. The tests with the lowest correlation (see Figure 5c) and prediction are those of ozonation and, in the case of catalytic ozonation, those with the highest dose of ozone applied. However, the PBRE predicts some tests satisfactorily, e.g.,  $[\text{O}_3]_{\text{T}} = 2.4 \text{ mg/min}$  with  $0.8 \text{ g/L FeOOH}$  and  $[\text{O}_3]_{\text{T}} = 6.4 \text{ mg/min}$  with  $0.8 \text{ g/L FeOOH}$ . The above results may indicate that the PBRE performs better in tests where catalytic activity is improved by increasing catalyst loading.

Figure 5c shows the generation of  $\text{OH}^\bullet$  calculated based on the PBRE model and the theoretical trends presented for catalytic ozonation. The generation of  $\text{OH}^\bullet$  can be observed as a function of the  $\text{FeOOH}$  load. Which shows that Goethite tends to improve the catalytic activity of ozone. In contrast, the test with  $[\text{O}_3]_{\text{T}} = 6.4 \text{ mg/min}$  and  $0.8 \text{ g/L}$  presented the highest theoretical generation of  $\text{OH}^\bullet$  compared to  $[\text{O}_3]_{\text{T}} = 6.4 \text{ mg/min}$  and  $0.8 \text{ g/L}$  of

FeOOH. This result is corroborated with the results of  $R_U$ , TOC, and degradation shown in Figure 2. It is important to note that after 8 min of operation, most tests begin to produce hydroxyl radicals for all the catalytic ozonation tests evaluated in this work.



**Figure 5.** Prediction of experimental data using the kinetic model elemental reactions for ozonation and catalytic ozonation (a,b), moles of  $OH^\bullet$  calculated (c), and correlation of experimental and calculated data (d).

The percentage correlation ( $R^2 = 0.69$ ) and percentage standard deviation ( $St_{y,x} = 0.56$ ) of calculated and experimental data obtained through the PBRE model present a lower prediction compared to the SSA and the second-order reaction kinetic model for the trends of the reaction rate of DCF during the ozonation and catalytic ozonation processes (see Figure 5d).

The PBRE mechanism approach allows the description of the transient evolution of the reaction kinetics. Besides, it facilitates the description of the variation of each of the intermediate species involved in the ozonation and catalytic ozonation process, without the need for drastic approximations or hypotheses on the kinetics and intermediate steps of chemical reactions [5].

#### 4.4. Sensitivity Analysis

Figure 6 shows the sensitivity analysis results for the kinetic parameters of two models that describe the reaction rate of DCF. The results obtained from the sensitivity analysis indicate that the indirect oxidation of DCF by  $OH^\bullet$  attacks is the kinetic parameter with the most significant contribution to the reaction kinetics of the ozonation and catalytic ozonation processes, both for the PBRE kinetic model with 94.9% and for the SSA with 91.67%. Additionally, the second kinetic parameter with the most significant influence on the reaction kinetics in the ozonation and catalytic ozonation processes during DCF

degradation is  $k_{O_3}$ , representing the direct attack reaction of ozone molecules to DCF (45.47% for PBRE and 7.77% for SSA).

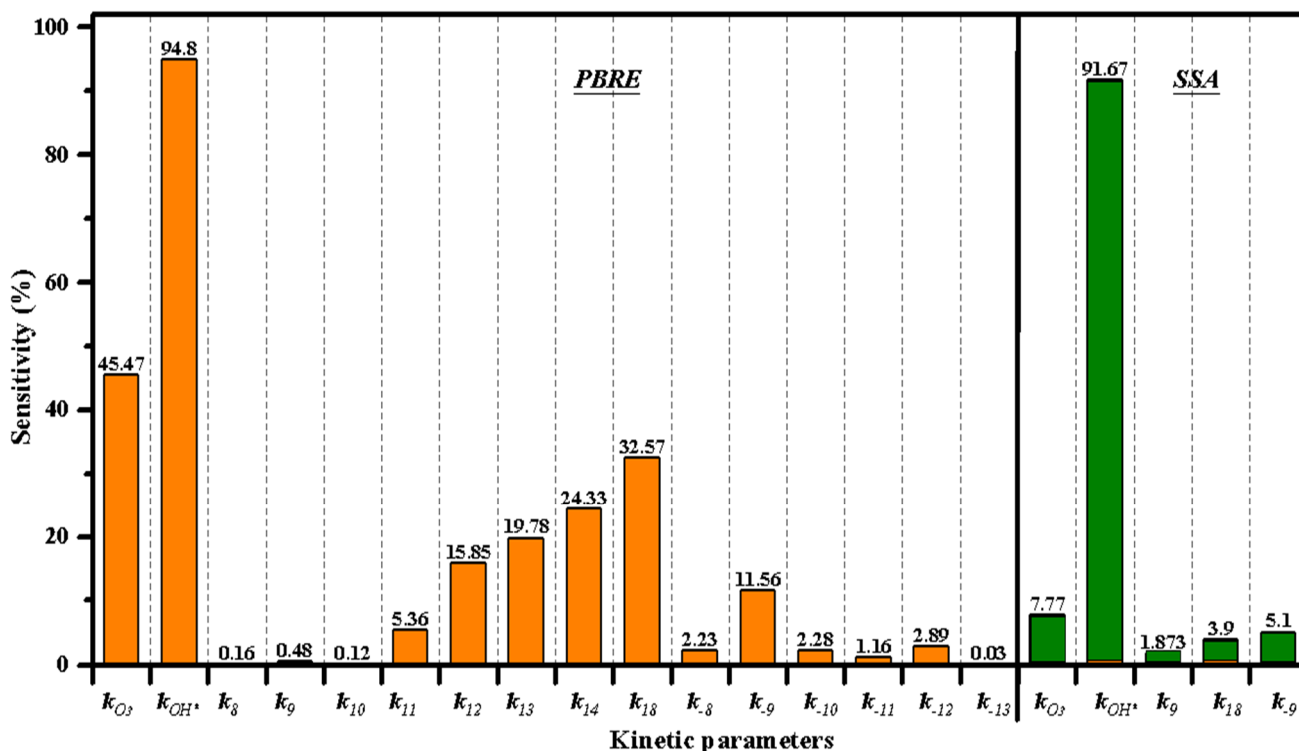


Figure 6. Sensitivity analysis for the proposal of kinetic models based on elemental reactions (cyan bar) and SSA (green bar).

The importance of  $OH^\bullet$  in the DCF degradation (indirect oxidation) is demonstrated by the magnitudes of  $k_{OH^\bullet}$  (previous sections). Moreover, the sensitivity analysis has also been corroborated by Guo et al. and Lara-Ramos et al. [24,51]. Similarly, numerous works reported in the literature have demonstrated the direct oxidation of DCF by direct attacks of the ozone molecule [6,10,24].

On the other hand, the sensitivity analysis also shows the importance of  $FeOOH$ , since, as can be seen in Figure 6, the kinetic parameters related to the adsorption and generation of  $OH^\bullet$  contribute to the reaction rate of catalytic ozonation with 32.57% and 24.33%, respectively, for the PBRE kinetic model. The importance of the catalytic activity of  $FeOOH$  in the decomposition of ozone and pollutant degradation has been reported in other works [14,20,33,39]. However, these results are for the SSA model. It is impossible to determine the importance of each elemental reaction by the set of masked parameters.

#### 4.5. Optimal Ozone Dosage and Catalyst Loading

Sensitivity analysis makes it possible to identify the appropriate and optimal kinetic parameters to adjust the DCF reaction kinetics in catalytic ozonation. These results are now used to project the optimal ranges of operating conditions, giving the best results in terms of DCF degradation (including TOC removal) from minimum ozone dose or catalyst loading values, as shown in Figure 7. For this, the results in DCF degradation have been plotted (see Figure 7a) for the nine catalytic ozonation experiments for the operational conditions, ozone dose, and  $FeOOH$  load presented in Table 3. The optimal operating conditions are projected to the extremes of  $[O_3]_T$  and load of  $FeOOH$ .



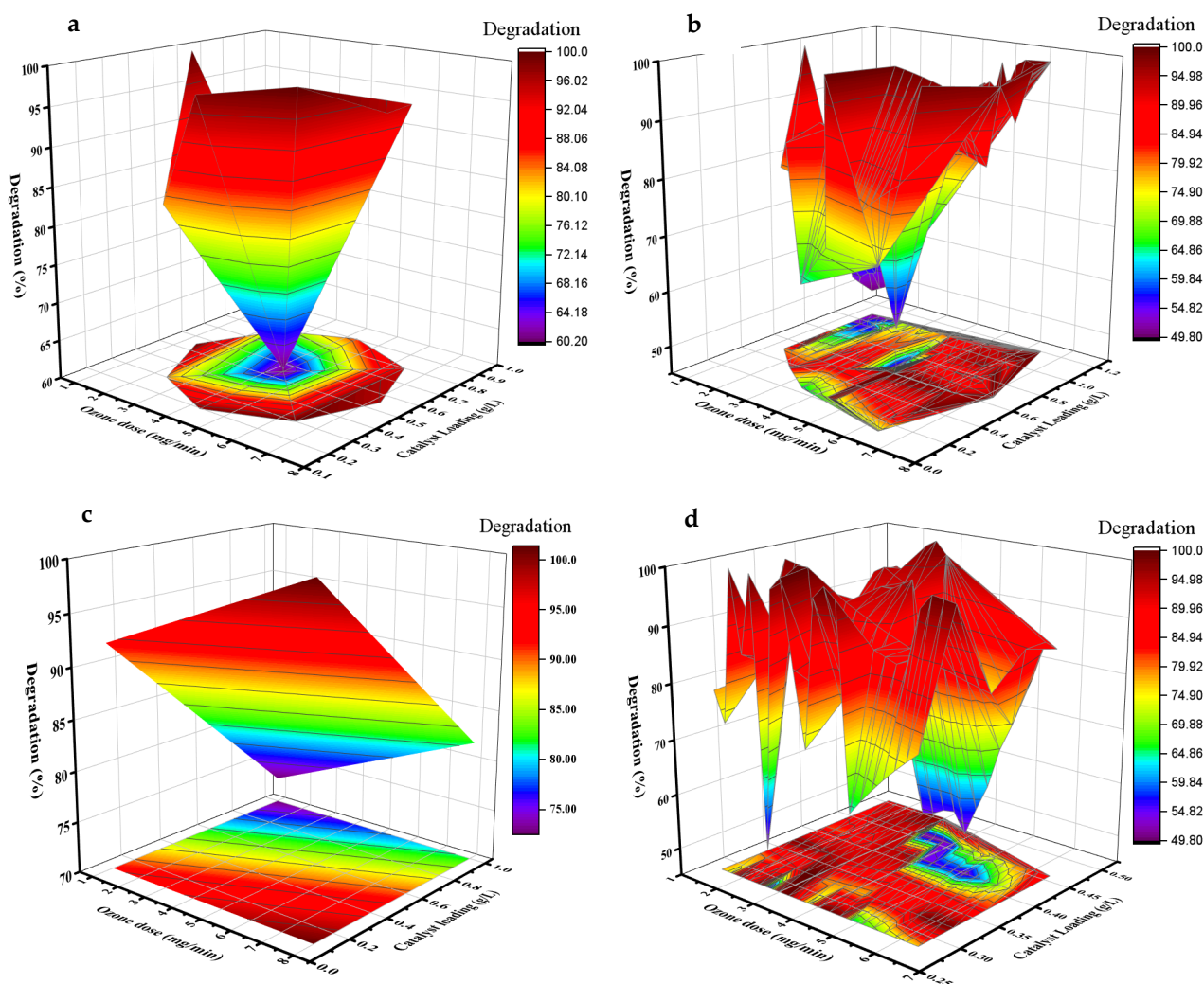


**Figure 7.** Ozone dose and suitable catalyst load according to a projection of experimental data (a), response surface (b), SSA model proposal (c), and PBRE model (d).

The response surface analysis for the operating conditions and percentages of DCF degradation indicates that the most significant operating parameter is the ozone dose. In contrast, the increase in the catalyst load can decrease the degradation percentages of DCF. The projection of a higher performance of DCF degradation with increasing ozone dose is a behavior reported by Lara-Ramos et al. [6], Moreira et al. [26], and Beltrán et al. [4].

On the other hand, the PBRE and SSA models were simulated with the adjusted parameters in the ozone dose intervals between 1.4 and 6.4 mg/min and catalyst loading between 0.2 and 0.8 g/L. The SSA model reveals the vital contribution when increasing  $[O_3]_T$  in the degradation of DCF. However, it also projects an essential contribution of the FeOOH load in catalytic ozonation. Additionally, the SSA model proposal indicates that the most appropriate dose to carry out catalytic ozonation should be greater than 4.5 mg/min.

Meanwhile, the projection of the PBRE model shows that there is a synergy between the ozone dose and the FeOOH load applied. This indicates the positive effect on DCF degradation of the ozone dose, but in the same way with doses 1.4–4 mg/min, the degradation percentage can be improved by increasing the FeOOH load. The above shows that Goethite has catalytic activity on ozone, which agrees with catalytic ozonation studies reported in the literature [38,39,42].

## 5. Conclusions

In this work, a kinetic study was developed with different reaction rate kinetic models for ozonation and catalytic ozonation processes. In addition, DCF as a model compound was degraded and mineralized by using an FC as a reagent system.

The study of the reaction rate under the kinetic approaches of pseudo-first-order, second-order, MORM, SSA, and PBRE demonstrate the vital contribution of the ozone molecule in DCF degradation. On the other hand, it is impossible to determine the contribution of  $\text{OH}^\bullet$  through kinetic models of pseudo-first-order, second-order, and MORM. However, they are frequently used to describe the reaction kinetics of the processes as a first approximation. Therefore, the SSA and PBRE kinetic models are fundamental to indicating the ozone molecule's importance and  $\text{OH}^\bullet$  on the degradation and mineralization of ECs such as DCF. This kinetic study theoretically demonstrated that ozone has a more significant contribution to DCF degradation (both in ozonation and catalytic ozonation). At the same time,  $\text{OH}^\bullet$  contributes and improves mineralization in catalytic ozonation.

The kinetic constants of reaction rate and their sensitivity analysis allow to identify the variables or operative factors of most significant importance in the processes of ozonation and catalytic ozonation, e.g., the ozone dose and  $\text{FeOOH}$  load. Additionally, the results obtained for the different kinetic approaches in this study allow to project the operating conditions with the highest performance in DCF degradation. Therefore, it allows to optimize the operating conditions in treating matrices or organic compounds present in water such as DCF.

Finally, this kinetic study of reaction rates illustrates the benefits of the flotation cell as a reactive system in future applications at the industrial level for the processes of ozonation and catalytic ozonation.

**Author Contributions:** Conceptualization, J.A.L.-R., M.A.M. and F.M.-M.; formal analysis, J.A.L.-R. and F.M.-M.; funding acquisition, F.M.-M. and J.A.L.-R.; investigation, J.A.L.-R. and M.A.F.A.; methodology, J.A.L.-R. and M.A.F.A.; project administration, M.A.M. and F.M.-M.; supervision, F.M.-M.; validation, J.A.L.-R. and M.A.F.A.; writing—original draft: J.A.L.-R.; writing—review and editing: J.A.L.-R., M.A.M. and F.M.-M. All authors have read and agreed to the published version of the manuscript.

**Funding:** Financial support from the Universidad del Valle, Universidad de Cartagena, ITSA and Minciencias (national doctoral program: 727 of 2015).

**Institutional Review Board Statement:** Not applicable.

**Informed Consent Statement:** Not applicable.

**Data Availability Statement:** Not applicable.

**Acknowledgments:** The authors thank the Administrative Department of Science, Technology, and Innovation of Colombia (Current Minciencias) for funding the national doctoral program (727 of 2015), Universidad del Valle, ITSA Institucion Universitaria, Universidad de Cartagena–Minciencias (Grant FP44842-128-2017), and the SENA (Grant No. 445-5455).

**Conflicts of Interest:** The authors declare no conflict of interest.

## Appendix A

### Appendix A.1. Physicochemical Properties of Drinking Tap Water in Cali, Valle del Cauca

**Table A1.** Physical and chemical parameters of drinking tape water Cali [6].

pH	uScm	Dissolved Solids (ppm)	Temperature (°C)
7.3 ± 0.03	150 ± 5	75 ± 5	28.5 ± 0.5

Cali environmental conditions: Environmental conditions of Cali: Average annual temperature: 25 °C, Relative humidity: 63%, and Atmospheric pressure: 1007 hPa, taken from <http://www.ideam.gov.co/web/tiempo-y-clima> (accessed on 6 May 2018).

### Appendix A.2. Experiment Design

In this research work, a central composite design was used to understand the interactions between critical parameters in terms of operating costs, such as ozone and FeOOH in the catalytic ozonation process. In addition, the central composite design optimizes the response in the degradation and mineralization of caffeine in a modified flotation cell (MFC).

The above is meant to provide greater control over the sensitivity of the variation and repeatability of the ozone concentration entered in the MFC. It was decided to use the percentage values indicated on the knob of the ozonator as a factor of change in the ozone concentration.

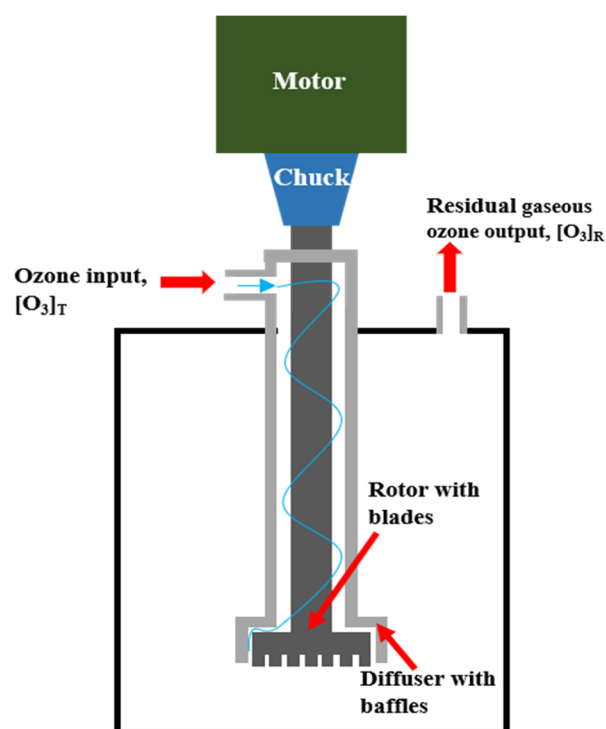


**Figure A1.** Diagram summarizing the system under which experiments were carried out. Extracted and adapted from [14].

On the other hand, in order to guarantee the standardization of the ozone concentrations entered, the ozone production was monitored before and after each experiment was performed.

**Table A2.** Design data for the modified flotation cell and ozonator.

Modified Flotation Cell		Ozonator	
Internal Volume	Hidrodynamic	External Dimensions	
Material: Duran Glass.	Stirring speed (rpm):	Material	
Height (m): 1.016	300–3300 rpm	Height (m)	0.35
Length (m): 0.61	Reaction volume (L): 0.44	Length (m)	0.381
Width (m): 0.991	Operational volume (L): 10	Width (m)	0.15
		Capacity (g/h)	5
		Ozone concentration (g/m <sup>3</sup> )	Adjustable from 47

### Appendix A.3. Proposal Model Based on Elementary Reactions (PBRE)

$$\frac{\partial[\text{DCF}]}{\partial t} = -k_{\text{O}_3}[\text{O}_3][\text{DCF}] - k_{\bullet\text{OH}}[\bullet\text{OH}][\text{DCF}] - k_{18}[\text{FeOOH}(\text{O}_3)][\text{DCF}] \quad (\text{A1})$$

$$\frac{d[O_3]}{dt} = -k_{O_3}[O_3][DCF] - k_1[O_3][OH^-] - k_2[O_3][HO_2^-] - k_4[O_3][O_2^- \bullet] - k_5[\bullet OH][O_3] - k_9[FeOOH][O_3] + k_{-9}[FeOOH(O_3)] - k_{11}[Fe(O)OH][O_3][H_2O] + k_{-11}[FeOH][\bullet OH][O_2^- \bullet][O_2][H^+] - k_{12}[O_3][FeOH] + k_{-12}[FeOH(O_3)] \quad (A2)$$

$$\frac{\partial[\bullet OH]}{\partial t} = -k_{\bullet OH}[\bullet OH][DCF] - k_5[\bullet OH][O_3] - k_6[HO_2^-][\bullet OH] - k_{-8}[\bullet OH][OH^-] + k_8[H_2O][O^- \bullet] + k_{11}[Fe(O)OH][O_3][H_2O] - k_{-11}[FeOH][\bullet OH][O_2^- \bullet][O_2][H^+] + k_{14}[FeO\bullet][H_2O] + k_{16}[HO_3\bullet] + k_{17}[O_3^- \bullet][H_2O] \quad (A3)$$

$$\frac{\partial[OH^-]}{\partial t} = -k_1[O_3][OH^-] + k_6[HO_2^-][\bullet OH] - k_{-8}[\bullet OH][OH^-] + k_8[H_2O][O^- \bullet] + k_{17}[O_3^- \bullet][H_2O] \quad (A4)$$

$$\frac{\partial[HO_2^-]}{\partial t} = +k_1[O_3][OH^-] - k_2[O_3][HO_2^-] - k_6[HO_2^-][\bullet OH] \quad (A5)$$

$$\frac{\partial[O_2]}{\partial t} = +k_1[O_3][OH^-] + k_4[O_3][O_2^- \bullet] + k_5[\bullet OH][O_3] + k_7[O_3^-] - k_{-7}[O_2][O^- \bullet] + k_{10}[FeOH(O_3)] - k_{-10}[Fe(O)OH][O_2] + k_{11}[Fe(O)OH][O_3][H_2O] - k_{-11}[FeOH][\bullet OH][O_2^- \bullet][O_2][H^+] + k_{16}[HO_3\bullet] + k_{17}[O_3^- \bullet][H_2O] \quad (A6)$$

$$\frac{\partial[HO_2\bullet]}{\partial t} = +k_2[O_3][HO_2^-] - k_3[HO_2\bullet] + k_{-3}[O_2^- \bullet][H^+] + k_5[O_3][OH\bullet] + k_6[HO_2^-][\bullet OH] \quad (A7)$$

$$\frac{\partial[O_3^- \bullet]}{\partial t} = +k_2[O_3][HO_2^-] + k_4[O_3][O_2^- \bullet] - k_7[O_3^- \bullet] + k_{-7}[O_2][O^- \bullet] + k_{15}[HO_3\bullet] - k_{-15}[H^+][O_3^- \bullet] - k_{17}[O_3^- \bullet][H_2O] \quad (A8)$$

$$\frac{\partial[O_2^- \bullet]}{\partial t} = +k_3[HO_2\bullet] - k_{-3}[O_2^- \bullet][H^+] - k_4[O_3][O_2^- \bullet] + k_{11}[Fe(O)OH][O_3][H_2O] - k_{-11}[FeOH][\bullet OH][O_2^- \bullet][O_2][H^+] \quad (A9)$$

$$\frac{\partial[H^+]}{\partial t} = +k_3[HO_2\bullet] - k_{-3}[O_2^- \bullet][H^+] + k_{11}[Fe(O)OH][O_3][H_2O] - k_{-11}[FeOH][\bullet OH][O_2^- \bullet][O_2][H^+] + k_{15}[HO_3\bullet] - k_{-15}[H^+][O_3^- \bullet] \quad (A10)$$

$$\frac{\partial[O^- \bullet]}{\partial t} = +k_7[O_3^- \bullet] - k_{-7}[O_2][O^- \bullet] + k_{-8}[\bullet OH][OH^-] - k_8[H_2O][O^- \bullet] \quad (A11)$$

$$\frac{\partial[H_2O]}{\partial t} = -k_8[H_2O][O^- \bullet] + k_{-8}[\bullet OH][OH^-] - k_{11}[Fe(O)OH][O_3][H_2O] + k_{-11}[FeOH][\bullet OH][O_2^- \bullet][O_2][H^+] - k_{14}[FeO\bullet][H_2O] - k_{17}[O_3^- \bullet][H_2O] \quad (A12)$$

$$\frac{\partial[FeOOH]}{\partial t} = -k_9[FeOOH][O_3] + k_{-9} \frac{k_9[FeOOH][O_3]}{k_{-9} + k_{18}[DCF]} \quad (A13)$$

$$\frac{\partial[FeOOH(O_3)]}{\partial t} = +k_9[FeOOH][O_3] - k_{-9}[FeOOH(O_3)] - k_{10}[FeOOH(O_3)] + k_{-10}[Fe(O)OH][O_2] - k_{18}[FeOOH(O_3)][DCF] \quad (A14)$$

$$\frac{\partial[Fe(O)OH]}{\partial t} = +k_{10}[FeOOH(O_3)] - k_{-10}[Fe(O)OH][O_2] - k_{11}[Fe(O)OH][O_3][H_2O] + k_{-11}[FeOH][\bullet OH][O_2^- \bullet][O_2][H^+] \quad (A15)$$

$$\frac{\partial[FeOH]}{\partial t} = +k_{11}[Fe(O)OH][O_3][H_2O] - k_{-11}[FeOH][\bullet OH][O_2^- \bullet][O_2][H^+] - k_{12}[O_3][FeOH] + k_{-12}[FeOH(O_3)] - k_{13}[FeOH] + k_{-13}[FeO\bullet][HO_3\bullet] + k_{14}[FeO\bullet][H_2O] \quad (A16)$$

$$\frac{\partial[FeOH(O_3)]}{\partial t} = +k_{12}[O_3][FeOH] - k_{-12}[FeOH(O_3)] \quad (A17)$$

$$\frac{\partial[\text{FeO}\bullet]}{\partial t} = +k_{13}[\text{FeOH}] - k_{-13}[\text{FeO}\bullet][\text{HO}_3\bullet] - k_{14}[\text{FeO}\bullet][\text{H}_2\text{O}] \quad (\text{A18})$$

$$\frac{d[\text{HO}_3\bullet]}{dt} = +k_{13}[\text{FeOH}] - k_{-13}[\text{FeO}\bullet][\text{HO}_3\bullet] - k_{15}[\text{HO}_3\bullet] + k_{-15}[\text{H}^+][\text{O}_3^-] - k_{16}[\text{HO}_3\bullet] + k_{-16}[\text{OH}\bullet][\text{O}_2] \quad (\text{A19})$$

$$\frac{d[\text{P}]}{dt} = +k_{\text{O}_3}[\text{O}_3][\text{DCF}] + k_{\bullet\text{OH}}[\bullet\text{OH}][\text{DCF}] + k_{18}[\text{FeOOH}(\text{O}_3)][\text{DCF}] \quad (\text{A20})$$

## References

- Gomes, J.; Costa, R.; Quinta-Ferreira, R.M.; Martins, R. Application of ozonation for pharmaceuticals and personal care products removal from water. *Sci. Total Environ.* **2017**, *586*, 265–283. [\[CrossRef\]](#)
- Verlicchi, P.; Al Aukidy, M.; Zambello, E. What have we learned from worldwide experiences on the management and treatment of hospital effluent?—An overview and a discussion on perspectives. *Sci. Total Environ.* **2015**, *514*, 467–491. [\[CrossRef\]](#)
- Rekhate, C.V.; Srivastava, J.K. Recent advances in ozone-based advanced oxidation processes for treatment of wastewater—A review. *Chem. Eng. J. Adv.* **2020**, *3*, 100031. [\[CrossRef\]](#)
- Beltrán, F.J.; Pocostales, P.; Alvarez, P.; Oropesa, A.L. Diclofenac removal from water with ozone and activated carbon. *J. Hazard. Mater.* **2009**, *163*, 768–776. [\[CrossRef\]](#)
- Beltrán, F.J. *Ozone Reaction Kinetics for Water and Wastewater Systems*, 1st ed.; Lewis, P.A., Ed.; CRC Press: London, UK, 2003; ISBN 1566706297.
- Lara-Ramos, J.A.; Sánchez-Gómez, K.; Valencia-Rincón, D.; Diaz-Angulo, J.; Mueses, M.; Machuca-Martínez, F. Intensification of the O<sub>3</sub>/TiO<sub>2</sub>/UV advanced oxidation process using a modified flotation cell. *Photochem. Photobiol. Sci.* **2019**, *18*, 920–928. [\[CrossRef\]](#)
- Verenitch, S.S.; Lowe, C.; Mazumder, A. Determination of acidic drugs and caffeine in municipal wastewaters and receiving waters by gas chromatography–ion trap tandem mass spectrometry. *J. Chromatogr. A* **2006**, *1116*, 193–203. [\[CrossRef\]](#) [\[PubMed\]](#)
- Almomani, F.A.; Shawaqfeh, M.; Bhosale, R.R.; Kumar, A. Removal of emerging pharmaceuticals from wastewater by ozone-based advanced oxidation processes. *Environ. Prog. Sustain. Energy* **2016**, *35*, 982–995. [\[CrossRef\]](#)
- Tiedeken, E.J.; Tahar, A.; McHugh, B.; Rowan, N.J. Monitoring, sources, receptors, and control measures for three European Union watch list substances of emerging concern in receiving waters—A 20 year systematic review. *Sci. Total Environ.* **2017**, *574*, 1140–1163. [\[CrossRef\]](#) [\[PubMed\]](#)
- Diaz-Angulo, J.; Lara-Ramos, J.; Mueses, M.; Hernández-Ramírez, A.; Puma, G.L.; Machuca-Martínez, F. Enhancement of the oxidative removal of diclofenac and of the TiO<sub>2</sub> rate of photon absorption in dye-sensitized solar pilot scale CPC photocatalytic reactors. *Chem. Eng. J.* **2020**, *381*, 122520. [\[CrossRef\]](#)
- Kohantorabi, M.; Moussavi, G.; Oulego, P.; Giannakis, S. Heterogeneous catalytic ozonation and peroxone-mediated removal of Acetaminophen using natural and modified hematite-rich soil, as efficient and environmentally friendly catalysts. *Appl. Catal. B Environ.* **2022**, *301*, 120786. [\[CrossRef\]](#)
- Araújo, A.; Soares, O.; Orge, C.; Gonçalves, A.; Rombi, E.; Cutrufello, M.; Fonseca, A.; Pereira, M.; Neves, I. Metal-zeolite catalysts for the removal of pharmaceutical pollutants in water by catalytic ozonation. *J. Environ. Chem. Eng.* **2021**, *9*, 106458. [\[CrossRef\]](#)
- Liu, B.; Ji, J.; Zhang, B.; Huang, W.; Gan, Y.; Leung, D.Y.; Huang, H. Catalytic ozonation of VOCs at low temperature: A comprehensive review. *J. Hazard. Mater.* **2022**, *422*, 126847. [\[CrossRef\]](#)
- Lara-Ramos, J.A.; Diaz-Angulo, J.; Machuca-Martínez, F. Use of modified flotation cell as ozonation reactor to minimize mass transfer limitations. *Chem. Eng. J.* **2021**, *405*, 126978. [\[CrossRef\]](#)
- Suwartha, N.; Syamzida, D.; Priadi, C.R.; Moersidik, S.S.; Ali, F. Effect of size variation on microbubble mass transfer coefficient in flotation and aeration processes. *Heliyon* **2020**, *6*, e03748. [\[CrossRef\]](#) [\[PubMed\]](#)
- Cardoso, J.C.; Bessegato, G.; Zanoni, M.V.B. Efficiency comparison of ozonation, photolysis, photocatalysis and photoelectrocatalysis methods in real textile wastewater decolorization. *Water Res.* **2016**, *98*, 39–46. [\[CrossRef\]](#)
- Chen, L.; Wang, H.; Sun, Y.; Zhao, Y.; Shi, H. Interface mechanisms of the catalytic ozonation of humic acids over siliceous ferrihydrite: Morphology, stability, and the catalytic process. *Environ. Res.* **2022**, *203*, 111870. [\[CrossRef\]](#) [\[PubMed\]](#)
- Jeirani, Z.; Soltan, J. Improved formulation of Fe-MCM-41 for catalytic ozonation of aqueous oxalic acid. *Chem. Eng. J.* **2017**, *307*, 756–765. [\[CrossRef\]](#)
- Lin, K.-Y.A.; Lin, T.-Y.; Chen, Y.-C.; Lin, Y.-F. Ferrocene as an efficient and recyclable heterogeneous catalyst for catalytic ozonation in water. *Catal. Commun.* **2017**, *95*, 40–45. [\[CrossRef\]](#)
- Wang, J.; Bai, Z. Fe-based catalysts for heterogeneous catalytic ozonation of emerging contaminants in water and wastewater. *Chem. Eng. J.* **2017**, *312*, 79–98. [\[CrossRef\]](#)
- Bai, Z.; Yang, Q.; Wang, J. Catalytic ozonation of sulfamethazine using Ce<sub>0.1</sub>Fe<sub>0.9</sub>OOH as catalyst: Mineralization and catalytic mechanisms. *Chem. Eng. J.* **2016**, *300*, 169–176. [\[CrossRef\]](#)

22. Pocostales, P.; Alvarez, P.; Beltrán, F. Catalytic ozonation promoted by alumina-based catalysts for the removal of some pharmaceutical compounds from water. *Chem. Eng. J.* **2011**, *168*, 1289–1295. [[CrossRef](#)]
23. Hu, M.; Yao, Z.; Hui, K.S. Novel mechanistic view of catalytic ozonation of gaseous toluene by dual-site kinetic modelling. *Chem. Eng. J.* **2017**, *308*, 710–718. [[CrossRef](#)]
24. Guo, Y.; Zhu, S.; Wang, B.; Huang, J.; Deng, S.; Yu, G.; Wang, Y. Modelling of emerging contaminant removal during heterogeneous catalytic ozonation using chemical kinetic approaches. *J. Hazard. Mater.* **2019**, *380*, 120888. [[CrossRef](#)]
25. Du, M.-S.; Chen, K.-P.; Lin, Y.-P. Degradation of ibuprofen and acetylsulfamethoxazole by multi-walled carbon nanotube catalytic ozonation: Surface properties, kinetics and modeling. *Environ. Sci. Water Res. Technol.* **2019**, *5*, 1758–1768. [[CrossRef](#)]
26. Moreira, N.F.; Orge, C.; Ribeiro, A.R.; Faria, J.; Nunes, O.; Pereira, M.F.; Silva, A.M. Fast mineralization and detoxification of amoxicillin and diclofenac by photocatalytic ozonation and application to an urban wastewater. *Water Res.* **2015**, *87*, 87–96. [[CrossRef](#)]
27. Lucas, M.S.; Reis, N.M.; Puma, G.L. Intensification of ozonation processes in a novel, compact, multi-orifice oscillatory baffled column. *Chem. Eng. J.* **2016**, *296*, 335–339. [[CrossRef](#)]
28. Graça, C.A.; Lima, R.B.; Pereira, M.F.R.; Silva, A.M.; Ferreira, A. Intensification of the ozone-water mass transfer in an oscillatory flow reactor with innovative design of periodic constrictions: Optimization and application in ozonation water treatment. *Chem. Eng. J.* **2020**, *389*, 124412. [[CrossRef](#)]
29. Aghaeinejad-Meybodi, A.; Ebadi, A.; Shafiei, S.; Khataee, A.; Kiadehi, A.D. Degradation of Fluoxetine using catalytic ozonation in aqueous media in the presence of nano- $\gamma$ -alumina catalyst: Experimental, modeling and optimization study. *Sep. Purif. Technol.* **2019**, *211*, 551–563. [[CrossRef](#)]
30. Arce-Sarria, A.; Caicedo-Rosero, C.L.; Lara-Ramos, J.A.; Diaz-Angulo, J.; Machuca-Martínez, F. Experimental data on synthesis and characterization of WO<sub>3</sub>/TiO<sub>2</sub> as catalyst. *Data Brief* **2019**, *25*, 104151. [[CrossRef](#)]
31. Lan, B.Y.; Nigmatullin, R.; Puma, G.L. Ozonation kinetics of cork-processing water in a bubble column reactor. *Water Res.* **2008**, *42*, 2473–2482. [[CrossRef](#)] [[PubMed](#)]
32. Lara-Ramos, J.; Saez, C.; Machuca-Martínez, F.; Rodrigo, M. Electro-ozonizers: A new approach for an old problem. *Sep. Purif. Technol.* **2020**, *241*, 116701. [[CrossRef](#)]
33. Lara-Ramos, J.A.; Constain-Escobar, A.M.; Rojas-Ortiz, K.V.; Diaz-Angulo, J.; Machuca-Martínez, F. A novel high rotation bubble reactor for the treatment of a model pollutant in ozone/goethite/H<sub>2</sub>O<sub>2</sub> and UV/goethite coupled processes. *Environ. Sci. Pollut. Res.* **2021**, *28*, 24079–24091. [[CrossRef](#)]
34. Lara-Ramos, J.A.; Llanos-Díaz, G.D.; Diaz-Angulo, J.; Machuca-Martínez, F. Evaluation of Caffeine Degradation by Sequential Coupling of TiO<sub>2</sub>/O<sub>3</sub>/H<sub>2</sub>O<sub>2</sub>/UV Processes. *Top. Catal.* **2020**, *63*, 1361–1373. [[CrossRef](#)]
35. Andreozzi, R.; Caprio, V.; Marotta, R.; Tufano, V. Kinetic modeling of pyruvic acid ozonation in aqueous solutions catalyzed by Mn(II) and Mn(IV) ions. *Water Res.* **2001**, *35*, 109–120. [[CrossRef](#)]
36. Hassani, A.; Khataee, A.; Karaca, S.; Fathinia, M. Heterogeneous photocatalytic ozonation of ciprofloxacin using synthesized titanium dioxide nanoparticles on a montmorillonite support: Parametric studies, mechanistic analysis and intermediates identification. *RSC Adv.* **2016**, *6*, 87569–87583. [[CrossRef](#)]
37. Zhang, T.; Ma, J. Catalytic ozonation of trace nitrobenzene in water with synthetic goethite. *J. Mol. Catal. A Chem.* **2008**, *279*, 82–89. [[CrossRef](#)]
38. Oputu, O.; Chowdhury, M.; Nyamayaro, K.; Fatoki, O.; Fester, V. Catalytic activities of ultra-small  $\beta$ -FeOOH nanorods in ozonation of 4-chlorophenol. *J. Environ. Sci.* **2015**, *35*, 83–90. [[CrossRef](#)]
39. Yan, P.; Shen, J.; Zhou, Y.; Yuan, L.; Kang, J.; Wang, S.; Chen, Z. Interface mechanism of catalytic ozonation in an  $\alpha$ -Fe<sub>0.9</sub>Mn<sub>0.1</sub>OOH aqueous suspension for the removal of iohexol. *Appl. Catal. B Environ.* **2020**, *277*, 119055. [[CrossRef](#)]
40. Cutler, P.; Gemperline, P.J.; de Juan, A. Experimental monitoring and data analysis tools for protein folding: Study of steady-state evolution and modeling of kinetic transients by multitechnique and multiexperiment data fusion. *Anal. Chim. Acta* **2009**, *632*, 52–62. [[CrossRef](#)] [[PubMed](#)]
41. Guo, X.; Minakata, D.; Niu, J.; Crittenden, J. Computer-Based First-Principles Kinetic Modeling of Degradation Pathways and Byproduct Fates in Aqueous-Phase Advanced Oxidation Processes. *Environ. Sci. Technol.* **2014**, *48*, 5718–5725. [[CrossRef](#)]
42. Pelalak, R.; Alizadeh, R.; Gharehabani, E. Enhanced heterogeneous catalytic ozonation of pharmaceutical pollutants using a novel nanostructure of iron-based mineral prepared via plasma technology: A comparative study. *J. Hazard. Mater.* **2020**, *392*, 122269. [[CrossRef](#)]
43. Yuan, L.; Shen, J.; Yan, P.; Zhang, J.; Wang, Z.; Zhao, S.; Chen, Z. Catalytic ozonation of 4-chloronitrobenzene by goethite and Fe<sup>2+</sup>-modified goethite with low defects: A comparative study. *J. Hazard. Mater.* **2019**, *365*, 744–750. [[CrossRef](#)]
44. Chen, J.; Tian, S.; Lu, J.; Xiong, Y. Catalytic performance of MgO with different exposed crystal facets towards the ozonation of 4-chlorophenol. *Appl. Catal. A Gen.* **2015**, *506*, 118–125. [[CrossRef](#)]
45. Sein, M.M.; Zedda, M.; Tuerk, J.; Schmidt, T.C.; Golloch, A.; Von Sonntag, C. Oxidation of Diclofenac with Ozone in Aqueous Solution. *Environ. Sci. Technol.* **2008**, *42*, 6656–6662. [[CrossRef](#)]
46. Hoigné, J. Chemistry of Aqueous Ozone and Transformation of Pollutants by Ozonation and Advanced Oxidation Processes. In *Quality and Treatment of Drinking Water II. The Handbook of Environmental Chemistry (Part C: Water Pollution)*; Hrubec, J., Ed.; Springer: Berlin/Heidelberg, Germany, 1998; Volume 5, pp. 83–141.

47. Evans, G.; Doroodchi, E.; Lane, G.; Koh, P.; Schwarz, M. Mixing and gas dispersion in mineral flotation cells. *Chem. Eng. Res. Des.* **2008**, *86*, 1350–1362. [[CrossRef](#)]
48. Amini, E.; Bradshaw, D.; Finch, J.; Brennan, M. Influence of turbulence kinetic energy on bubble size in different scale flotation cells. *Miner. Eng.* **2013**, *45*, 146–150. [[CrossRef](#)]
49. Malik, S.N.; Ghosh, P.C.; Vaidya, A.N.; Mudliar, S.N. Hybrid ozonation process for industrial wastewater treatment: Principles and applications: A review. *J. Water Process. Eng.* **2020**, *35*, 101193. [[CrossRef](#)]
50. He, H.; Liu, Y.; Wu, D.; Guan, X.; Zhang, Y. Ozonation of dimethyl phthalate catalyzed by highly active Cu O-Fe<sub>3</sub>O<sub>4</sub> nanoparticles prepared with zero-valent iron as the innovative precursor. *Environ. Pollut.* **2017**, *227*, 73–82. [[CrossRef](#)]
51. Guo, Y.; Wang, H.; Wang, B.; Deng, S.; Huang, J.; Yu, G.; Wang, Y. Prediction of micropollutant abatement during homogeneous catalytic ozonation by a chemical kinetic model. *Water Res.* **2018**, *142*, 383–395. [[CrossRef](#)]